International Journal of Heat and Mass Transfer 117 (2018) 1352–1367

Contents lists available at ScienceDirect

International Journal of Heat and Mass Transfer

journal homepage: www.elsevier.com/locate/ijhmt

Review

Pool boiling critical heat flux (CHF) – Part 1: Review of mechanisms, models, and correlations

Gangtao Liang [a,b], Issam Mudawar [b,*]

[a] Key Laboratory of Ocean Energy Utilization and Energy Conservation of Ministry of Education, School of Energy and Power Engineering, Dalian University of Technology, Dalian 116024, China
[b] Purdue University Boiling and Two-Phase Flow Laboratory (PU-BTPFL), School of Mechanical Engineering, 585 Purdue Mall, West Lafayette, IN 47907, USA

ARTICLE INFO

Article history:
Received 12 July 2017
Received in revised form 29 September 2017
Accepted 29 September 2017
Available online 2 November 2017

Keywords:
Pool boiling
Critical heat flux (CHF)
Surface orientation
Contact angle

ABSTRACT

Critical heat flux (CHF) is arguably the most important design and safety parameter for any heat-flux controlled boiling application. The present two-part study is focused on CHF for pool boiling from flat surfaces. The first part will review different CHF models and associated mechanisms and parametric trends, while the second part will be dedicated to assessment of CHF models and correlations. Aside from Kutateladze's 1948 pioneering CHF formulation, which is based on dimensional analysis, five different CHF mechanisms are prevalent in the literature: bubble interference, hydrodynamic instability, macrolayer dryout, hot/dry spot, and interfacial lift-off. Additionally, many modifications to these mechanisms have been proposed to improve predictive accuracy in tackling the parametric influences of pressure, surface size and roughness, surface orientation, and contact angle. Among the five mechanisms, Zuber's hydrodynamic instability theory has received the most attention because of both its mechanistic formulation and theoretical appeal. More recently, the interfacial lift-off mechanism, which is also theoretically based, has received significant experimental validation, and offers the advantage of tackling different surface orientations. Overall, it is shown that, despite the large body of published pool boiling CHF literature, there are major data gaps in the coverage of relevant parameters. This points to a need for more strategically planned future experiments that would also include microphotographic analysis of near-wall interfacial features, in order to validate or dispute proposed CHF mechanisms.

Contents

* Corresponding author.
E-mail address: mudawar@ecn.purdue.edu (I. Mudawar).
URL: https://engineering.purdue.edu/BTPFL (I. Mudawar).

https://doi.org/10.1016/j.ijheatmasstransfer.2017.09.134
0017-9310/

Nomenclature

A	area
A_g	area occupied by vapor jets
A_w	total surface area
c_p	specific heat at constant pressure
d	bubble diameter
D_j	vapor column (jet) diameter
f	bubble departure frequency
f_i	interfacial friction factor
g	gravitational acceleration
H	wall thickness
h_{fg}	latent heat of vaporization
K	dimensionless critical heat flux
k	thermal conductivity; empirical parameter
L	heater length
P	pressure
P_c	critical pressure
Pr	Prandtl number
q''	heat flux
q''_{CHF}	critical heat flux
q''_l	localized heat flux; wetting front heat flux
R	vapor stem radius
r	radius of curvature of interface
R_a	surface roughness
R_i	individual gas constant
S	thermal activity parameter
S_m	mean spacing between surface roughness peaks
T	temperature
t	time
ΔT_{sat}	surface superheat, $T_w - T_{sat}$
ΔT_{sub}	liquid subcooling, $T_{sat} - T_f$
u	velocity

Greek symbols

α	contact angle
δ	macrolayer thickness; vapor layer thickness
δ_*	linear scale of capillary disturbance
θ	surface orientation angle measured from horizontal, upward-facing orientation
λ	wavelength
λ_c	critical wavelength of Taylor instability; critical wavelength of Helmholtz instability
λ_d	most dangerous wavelength of Taylor instability
λ_H	wavelength of Helmholtz instability
λ_T	wavelength of Taylor instability
μ	dynamic viscosity
υ	kinematic viscosity
ρ	density
σ	surface tension
τ	bubble hovering time

Subscripts

asy	asymptotic
c	critical
d	most dangerous
f	liquid
g	vapor; gas
H	Helmholtz
h	high
j	jet
l	low
max	maximum
sat	saturation
sub	subcooling
T	Taylor
w	surface

1. Introduction

1.1. Pool boiling applications

The past four decades have witnessed unprecedented increases in rate of heat dissipation in a number of technologies, coupled with a trend for smaller and more lightweight system architectures. Responding to these trends, a variety of two-phase thermal management techniques have been proposed [1,2]. These techniques have been the focus of extensive studies at the Purdue University Boiling and Two-Phase Flow Laboratory (PU-BTPFL) spanning over three decades. They include passive (pump-free) cooling schemes, including both capillary-driven devices (heat pipes, capillary pumped loops, and loop heat pipes) [3] and pool

boiling thermosyphons [4]. On the other hand, a liquid pump is required for more demanding situations to capitalize on the heat transfer enhancement resulting from faster fluid motion, using such schemes as falling film [5], channel flow boiling [6–8], mini/micro-channel flow boiling [9–12], jet-impingement [13], and spray [14,15], as well as hybrid cooling schemes combining the merits of mini/micro-channel flow and jet impingement [16]. Key to implementing any of these schemes is the ability to predict boiling performance, especially critical heat flux (CHF). The present study is focused entirely on CHF prediction for pool boiling.

Aside from being the simplest and most cost effective of all two-phase cooling schemes, pool boiling is the most prevalent and most mature in industry, and is found in both low temperature and high temperature applications. Examples of the former include cooling of electronic components, power devices, and superconductor coils, where pool boiling capitalizes upon the coolant's sensible and latent heat to facilitate removal of large amounts of heat while maintaining device temperatures safely below limits dictated by both material and device reliability constraints. A prime example of high temperature applications is quenching of metal alloy parts from very high temperatures to achieve optimum alloy microstructure and superior mechanical properties.

1.2. Boiling curve

Pool boiling heat transfer mechanisms and regimes are described with the aid of the boiling curve [17,18], as shown in Fig. 1. This curve depicts the variations of heat flux from the surface to a pool of liquid with wall superheat (wall temperature minus liquid saturation temperature). It is highly effective at identifying the different heat transfer regimes encountered at different levels of wall superheat. They are comprised of (a) the single-phase regime, corresponding to low superheats, (b) nucleate boiling regime, associated with bubble nucleation at the surface, (c) transition boiling regime, where portions of the surface encounter bubble nucleation while other regions are blanketed with vapor, and (d) film boiling regime, corresponding to high wall superheats that cause vapor blanketing over the entire surface. These four regimes are demarcated by three important transition points: (i) onset of boiling (or incipient boiling) corresponding to first bubble formation on the surface, (ii) critical heat flux (CHF), where bubble nucleation in nucleate boiling is replaced by localized vapor blankets merging together across the surface, and (iii) minimum heat flux (or Leidenfrost point), corresponding to the onset of breakup of the continuous vapor blanket in film boiling when decreasing wall superheat. These transition points mark profound changes in heat transfer effectiveness between the different regimes, with the nucleate boiling regime providing the highest heat transfer coefficients and the film boiling regime the lowest.

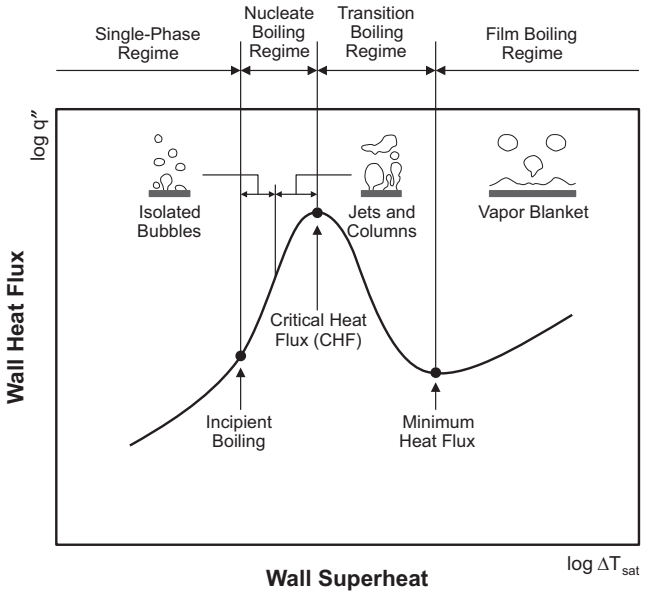

Fig. 1. Pool boiling curve.

The present study is focused entirely on CHF, which is arguably the most important design and safety parameter in pool boiling. For heat flux controlled cooling applications, exceeding CHF triggers a rapid and unsteady transition from highly efficient nucleate boiling to very heat transfer deficient film boiling. It is also accompanied by a sharp increase in surface temperature that may lead to physical damage, meltdown, or burnout of the surface, which is why CHF occurrence is often referred to as 'boiling crisis.' From a practical point of view, optimum cooling is achieved by maintaining conditions within the nucleate boiling regime, above the onset of boiling, but safely below CHF. Given the great importance of CHF to cooling system design, investigators have studied its mechanisms for decades in pursuit of predictive models and correlations.

1.3. Trigger mechanisms of CHF

Five different mechanisms for pool boiling CHF are prevalent in the literature: *bubble interference* [19], *hydrodynamic instability* [20], *macrolayer dryout* [21], *hot/dry spot* [22,23], and *interfacial lift-off* [24]. Among the five mechanisms, the theory of hydrodynamic instability by Zuber [20] has attracted the most attention, being the first theoretical and mechanistic CHF model. In fact, the majority of published pool boiling CHF studies consist of efforts to improve the predictive capability of the Zuber model by accounting for parametric effects not captured in the original model. This paper will review the five CHF mechanisms using the schematic in Fig. 2 as guide for the nomenclature adopted in the review.

1.4. Kutateladze's CHF formulation based on dimensional analysis

Before discussing the different CHF mechanisms, it is important to highlight an early pioneering investigation that led to the popular CHF formulation adopted later by many investigators. In 1948, Kutateladze [25–27] addressed pool boiling CHF prediction using dimensional analysis. He postulated that CHF occurrence is dictated by the relative influences of vapor inertia, surface tension, and buoyancy. He described vigorous boiling at the surface as taking place in the form of vapor jets that release vapor perpendicular to the surface at velocity u_g, which is expressed as

$$u_g = \frac{q''}{\rho_g h_{fg}}, \tag{1}$$

where q'', ρ_g, and h_{fg} are the heat flux, vapor density, and latent heat of vaporization, respectively. At CHF, Kutateladze described kinetic energy of the vapor as separating the liquid from the surface by just balancing the opposing gravitational force acting on the suspended liquid,

$$\rho_g u_g^2 \sim g(\rho_f - \rho_g)\delta_*, \tag{2}$$

where g and ρ_f represent gravitational acceleration and liquid density, respectively, and δ_* the linear scale of capillary disturbances, expressed as

$$\delta_* = \left[\frac{\sigma}{g(\rho_f - \rho_g)}\right]^{1/2}, \tag{3}$$

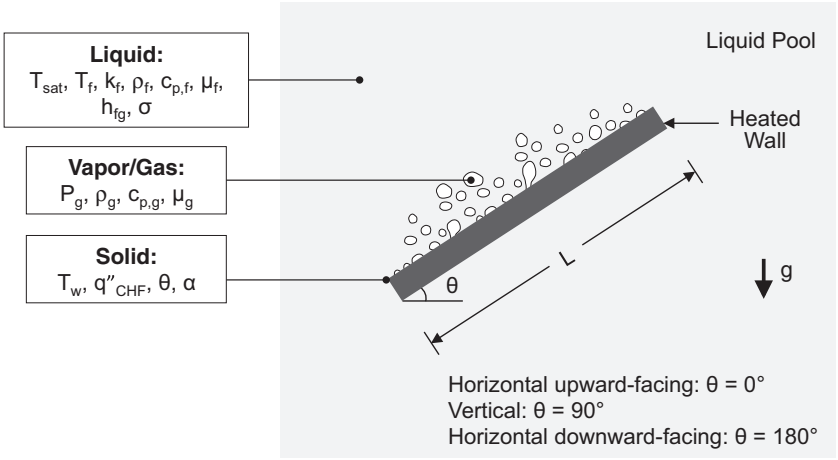

Fig. 2. Schematic of pool boiling and relevant nomenclature.

σ being the surface tension. Substituting Eqs. (1) and (3) into Eq. (2) yields Kutateladze's well-known CHF relation

$$\frac{q''_{CHF}}{\rho_g h_{fg}[\sigma g(\rho_f-\rho_g)/\rho_g^2]^{1/4}} = K, \tag{4}$$

where K is a constant and hereafter referred to as dimensionless CHF. The value of $K = 0.16$ was recommended by Kutateladze for pool boiling on a large horizontal flat surface. Note that because this equation was derived from dimensional analysis premises, it is expected that different theoretical CHF models for saturated pool boiling may be arranged into the form of Eq. (4), independent of the CHF mechanism proposed.

1.5. Objectives of study

This paper is the first part of a two-part study addressing pool boiling CHF. The present part will review CHF models and correlations based on different 'trigger' mechanisms, and is limited to flat and smooth surfaces, and pure liquids, and excludes modified surfaces and liquids with nanoparticles, surfactants, or soluble salts. The review will also be focused on CHF corresponding to steady state and saturated and/or near saturated conditions. The second part of this study [28] will assess the accuracy of available pool boiling CHF models and correlations against a new database amassed by the present authors from different sources. It is important to mention an article by Arik et al. [29], which reviewed pool boiling CHF studies prior to 2011, but was focused on CHF enhancement methodologies, rather than on mechanisms and models. Unlike the prior review, the present study concerns CHF mechanisms, models, and correlations, as well as parametric influences of pressure, surface size and thermal properties, surface roughness, contact angle, and liquid viscosity.

2. Rohsenow and Griffith bubble interference model

In 1955, Rohsenow and Griffith [19] proposed a model for pool boiling CHF based on the trigger mechanism of bubble interference. The model describes initially isolated spherical vapor bubbles touching one another in tight formation, and postulates that CHF will occur when neighboring bubbles coalesce radially, causing coverage of the surface with vapor. The model was represented by the relation

$$q''_{CHF} = 0.012\,\rho_g h_{fg}\left(\frac{\rho_f-\rho_g}{\rho_g}\right)^{0.6}. \tag{5}$$

Chang and Snyder [30] proposed a different mechanism, which, like that of Rohsenow and Griffith, is based on isolated bubble interference,

$$q''_{CHF} = \frac{1}{2}\left(\frac{\pi}{6}\right)^{5/6}(0.0119\alpha)^{1/2}\rho_g h_{fg}\left[2\sigma g(\rho_f-\rho_g)/\rho_g^2\right]^{1/4}, \tag{6}$$

where α is the contact angle. Notice that Eq. (6) has the same form as Kutateladze's Eq. (4).

It is important to note that Eqs. (5) and (6) are both based on bubble interference of isolated bubbles, which, as will be discussed later, contradicts findings from many later high-speed photographic studies that point to bubble coalesce occurring well prior to CHF.

3. Zuber hydrodynamic instability model

3.1. Zuber model

Inspired by Kutateladze's work, Zuber [20,31] constructed a model for CHF in saturated pool boiling on an infinite flat surface based on hydrodynamic instability theory. A follow-up study by Zuber et al. [32] provided further details of the original model. Notice that different variations of the Zuber model have been proposed over the years. Following is the most complete formulation of the model.

As indicated in the schematic in Fig. 3(a), just prior to CHF occurrence, vapor columns or jets emanate at mean velocity u_g perpendicular to and away from the surface, as the surface is being replenished by liquid flowing between the jets and towards the surface at velocity u_f. The surface can be modeled as consisting of repeated square cells, Fig. 3(b), each consisting of a single jet and surrounding liquid. Zuber further assumed that the vapor jets are formed along the surface by the Taylor instability, acquiring a jet diameter $D_j = \lambda_T/2$, where λ_T is the Taylor wavelength, the value of which lies between the 'critical wavelength', λ_c, and the 'most dangerous wavelength', λ_d, which are expressed, respectively, as

$$\lambda_c = 2\pi\sqrt{\frac{\sigma}{g(\rho_f-\rho_g)}} \tag{7a}$$

and

$$\lambda_d = \sqrt{3}\,\lambda_c = 2\pi\sqrt{3}\sqrt{\frac{\sigma}{g(\rho_f-\rho_g)}}. \tag{7b}$$

Therefore, the ratio of surface area occupied by the jets, A_g, to the total surface area, A_w, is identical to that for a single cell.

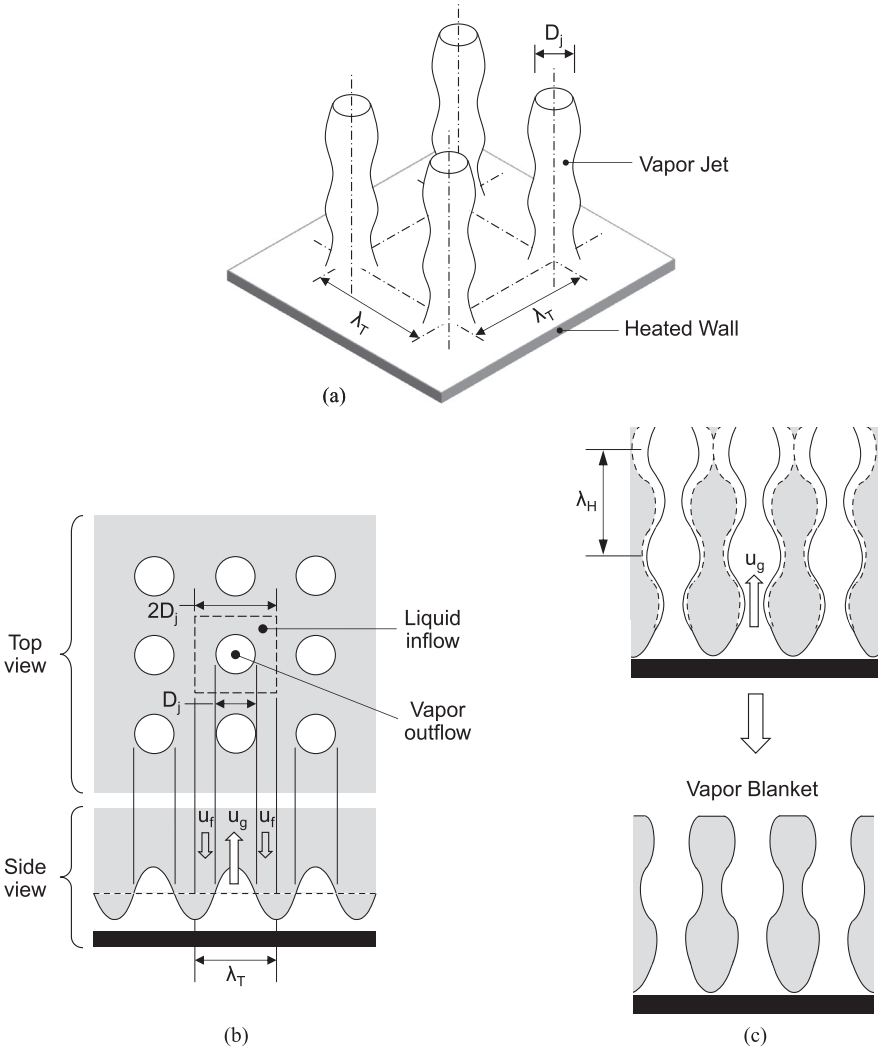

Fig. 3. Schematic of the Zuber hydrodynamic instability model. (a) Vapor jet formation prior to CHF. (b) Unit cell containing a single jet and surrounding liquid. (c) Vapor mushroom formation due to Helmholtz instability.

$$\frac{A_g}{A_w} = \frac{\pi \frac{(\lambda_T/2)^2}{4}}{\lambda_T^2} = \frac{\pi}{16}. \tag{8}$$

Also, just prior to CHF occurrence, the vapor and liquid velocities are related by continuity, which can be combined with Eq. (8) to yield

$$u_f = \frac{\rho_g A_g u_g}{\rho_f (A_w - A_g)} = \frac{\rho_g}{\rho_f}\left(\frac{A_g/A_w}{1 - A_g/A_w}\right) u_g = \frac{\rho_g}{\rho_f}\left(\frac{\pi}{16 - \pi}\right) u_g. \tag{9}$$

Assuming that the heat generated from the surface at CHF is consumed entirely by vaporization of the liquid, CHF can be related to the vapor velocity according to

$$q''_{CHF} = (A_g/A_w)\rho_g h_{fg} u_g. \tag{10}$$

Combining the above equation with Eq. (8) gives the following expression for the vapor velocity.

$$u_g = \frac{q''_{CHF}}{\left(\frac{\pi}{16}\right) \rho_g h_{fg}}. \tag{11}$$

The next step in the model constitutes the trigger mechanism for CHF. Because of velocity differences between the vapor and liquid, the interface of the vapor jet incurs Helmholtz instability, and growth of this instability causes merging of adjacent vapor jets, Fig. 3(c), giving rise to formation of the vapor mushroom responsible for preventing any further liquid from replenishing the surface. The Helmholtz instability can be expressed as

$$u_g - (-u_f) = \left(\frac{\rho_f + \rho_g}{\rho_f \rho_g}\right)^{1/2} \left(\frac{2\pi\sigma}{\lambda_H}\right)^{1/2}, \tag{12}$$

where λ_H is the critical Helmholtz wavelength. Zuber assumed that the vapor jet diameter is related λ_H by the relation

$$\lambda_H = \pi D_j. \tag{13}$$

Combining Eqs. (7a)-(13) yields

$$\frac{q''_{CHF}}{\rho_g h_{fg} [\sigma g (\rho_f - \rho_g)/\rho_g^2]^{1/4}} = \left[\left(\frac{\pi}{24}\frac{3}{\sqrt{2\pi}}\frac{1}{3^{1/4}}\right) \rightarrow \left(\frac{\pi}{24}\frac{3}{\sqrt{2\pi}}\right)\right] \left[\frac{\left(\frac{\rho_f + \rho_g}{\rho_f}\right)^{1/2}}{1 + \frac{\rho_g}{\rho_f}\frac{\pi}{16-\pi}}\right]. \tag{14}$$

Notice that the range indicated in the first bracket to the right of Eq. (14) is the result of assuming $\lambda_c < \lambda_T < \lambda_d$. Excluding pressures near critical (*i.e.*, $\rho_g \ll \rho_f$), the right hand side of Eq. (14) can be

simplified into a numerical value ranging from 0.119 and 0.157. Zuber recommended an intermediate value of 0.131, which leads to the following final form of the model,

$$\frac{q''_{CHF}}{\rho_g h_{fg}\left[\sigma g(\rho_f-\rho_g)/\rho_g^2\right]^{1/4}} = K = 0.131. \tag{15}$$

It is important to note that Zuber's model has achieved great success in predicting pool boiling CHF data, becoming the most prevalent CHF model published thus far. Because of the pioneering efforts of Kutateladze and Zuber and similar dimensionless CHF representations, Eq. (4) is often referred to as the *Kutateladze-Zuber equation*. Many attempts have been made to modify Zuber's original model to account for various additional effects, such as surface size, shape, and orientation, contact angle, and liquid viscosity, which will be discussed in detail in the following sections.

3.2. Modifications to Zuber's model for horizontal, upward-facing orientation

3.2.1. Effects of wall size, thickness, and thermal properties

Lienhard and Dhir [33,34] modified Zuber's model by setting $\lambda_H = \lambda_d$ instead of Zuber's $\lambda_H = \pi D_j$ [20,31]. This modification lead to a 14% increase in CHF,

$$q''_{CHF}/q''_{CHF,Zuber} = 1.14. \tag{16}$$

They also measured CHF for different surface sizes and reported that the infinite flat surface assumption is fairly accurate for surface widths greater than $3\lambda_d$ [35]. Lu et al. [36] also modified Zuber's model by accounting for nucleation site density and finite heater size. Pezo and Stevanovic [37] investigated the effects of nucleation site density on CHF numerically with the aid of the two-fluid model. Zhang et al. [38] used 2D simulations of pool boiling and concluded that the surface can be treated as infinite when the ratio of heater width to capillary length is greater than 12. Chang [39] suggested a CHF ratio of 0.75 for vertical to horizontal surface orientations, and obtained a CHF relation similar in form to Eq. (15).

Tachibana et al. [40], Golobič and Bergles [41], Ferjančič and Golobič [42], and Gogonin [43] all reported that hydrodynamic instability theory alone is insufficient for a generalized CHF model. They suggested surface parameters, such as wall thickness, thermal conductivity, and chemistry, can also have appreciable influences on CHF. More specifically, a wall thickness threshold value must be exceeded in order to achieve values similar to those predicted by Zuber, and thinner walls produce smaller CHF values. Tachibana et al. found that CHF correlates well with the wall's heat capacity per unit heat transfer area, and a thickness of at least 0.8 mm is necessary for a stainless steel wall to be free from heat capacity effects. Grigoriev et al. [44] showed experimentally that CHF for a copper wall in liquid helium increases asymptotically up to a thickness of 0.35 mm. Gogonin [45] found that a width of 2 capillary lengths is sufficient to eliminate the length scale effects. Bar-Cohen and McNeil [46] employed a 'thermal activity' parameter, $S = H\sqrt{(\rho c_p k)_w}$, to address the effects of wall thickness, H, as well as the wall's density, ρ_w, specific heat, $c_{p,w}$, and thermal conductivity, k_w. They found that the effects of S on CHF data for horizontal sputtered platinum and doped silicon surfaces in dielectric liquids can be correlated according to

$$\frac{q''_{CHF}}{q''_{CHF,asy}} = \frac{S}{S+0.8}, \tag{17}$$

where $q''_{CHF,asy}$ is the asymptotic CHF for thick walls. This relationship yields 90% of asymptotic CHF for $S = 8$ and 99% for $S = 85$. Follow-up work by Watwe and Bar-Cohen [47] (referred to by Arik and Bar-Cohen [48]) modified this relationship into

$$\frac{q''_{CHF}}{q''_{CHF,asy}} = \frac{S}{S+0.1}, \tag{18}$$

which yields 90% of asymptotic CHF for $S = 1$ and 99% for $S = 10$. Watwe and Bar-Cohen also used Eq. (18) to develop a composite relation for pool boiling CHF that accounts for both hydrodynamic and conduction effects, in addition to the effects of pressure, subcooling, and surface length,

$$K = \frac{\pi}{24}\left(\frac{S}{S+0.1}\right)\left\{1+\left(0.3014-0.01507L\sqrt{\frac{g(\rho_f-\rho_g)}{\sigma}}\right)\right\} \times\left\{1+0.03\left[\left(\frac{\rho_f}{\rho_g}\right)^{3/4}\frac{c_{p,f}}{h_{fg}}\right]\Delta T_{sub}\right\}. \tag{19}$$

Golobič and Bergles [41] provided an alternative correlation accounting for the wall conduction effects based on experimental data for saturated FC-72,

$$\frac{q''_{CHF}}{q''_{CHF,asy}} = 1-\exp\left[-\left(\frac{S}{2.44}\right)^{0.8498}-\left(\frac{S}{2.44}\right)^{0.0581}\right]. \tag{20}$$

A more recent study by Bombardieri and Manfletti [49] demonstrated the effects of wall material on CHF, and their CHF data were overestimated for aluminum but underestimated for stainless steel when using Eq. (16) of Lienhard and Dhir [33,34]. Jergel and Stevenson [50] also examined the effects of wall material by comparing CHF data for aluminum and copper.

3.2.2. Effects of contact angle

Note that the Kutateladze-Zuber equation is independent of surface conditions. Despite validation of this independence by Bewilogua et al. [51], many disagree with this assessment and point to lack of surface effects as basis for disproving the hydrodynamic instability mechanism.

Stock [52] reported that contact angle, α, has a weak influence on CHF. O'Hanley et al. [53] also found that wettability alone has little influence on CHF for smooth surfaces. However, as shown in Fig. 4, Gaertner [54], Costello and Frea [55], Maracy and Winterton [56], and Hahne and Diesselhorst [57] all found that CHF decreases appreciably with decreasing surface wettability.

Recently, pool boiling CHF enhancements by nanoparticle thin-film coatings, porous layers, and with nanofluids were also attributed to increased wettability [58–61] (details of which can be found in review articles by Mori and Utaka [62], Ciloglu and Bolukbasi [63], and Fang et al. [64]). Truong et al. [65] also emphasized the important influence of wettability on CHF. Liaw and Dhir [66]

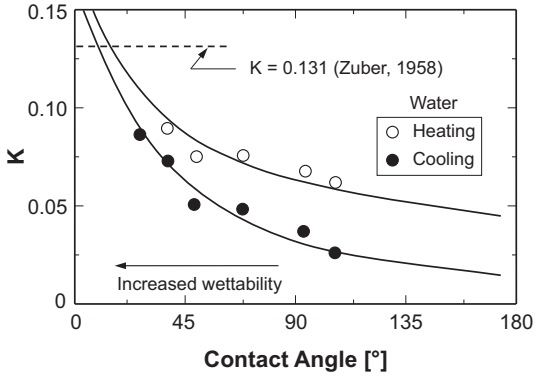

Fig. 4. Contact angle effects on dimensionless CHF for water. Adapted from Liaw and Dhir [66].

reported that CHF for a contact angle of 107° is only half that predicted by hydrodynamic instability theory.

The contact angle/wettability effects on CHF were also incorporated into models or empirical correlations by Kirichenko and Chernyakov [67], Ramilison et al. [68], Kandlikar [69], Liao et al. [70], and Phan et al. [71]. However, Liao et al. [70] cautioned that it is difficult to establish a robust relation between CHF and contact angle because of synchronous variations in thermal properties of both fluid and surface with temperature that can influence contact angle greatly.

It can therefore be concluded that contact angle is important to modeling pool boiling CHF even for smooth surfaces, let alone the complicated contact angle variations resulting from external influences [72]. This fact points to a need for more systematic studies of pool boiling CHF from smooth surfaces.

3.2.3. Effects of surface roughness

O'Hanley et al. [53], Berenson [73], Lyon [74], Ramilison and Lienhard [75], and Nishio and Chandratilleke [76] indicated that CHF is independent of surface roughness. However, Bailey et al. [77] obtained CHF values higher than those predicted by Eq. (15), and attributed this increase to surface roughness effects. Using pentane, hexane, and FC-72, Guan et al. [78] examined CHF on surfaces with root mean square roughness values between 0.15 and 5 μm, and reported up to 15% CHF enhancement with the 5-μm surface compared to the smooth surface. Kim et al. [79] found a strong dependence of water CHF on surface roughness for copper surfaces with moderate wettability of $\alpha = 60–70°$. CHF increased from 77.5 W/cm^2 for a smooth surface with $R_a = 0.041$ μm to 162.5 W/cm^2 for a rough surface with $R_a = 2.36$ μm, which was ascribed to capillary wicking effects on the rougher surface. They also proposed the following correlation to account for these effects,

$$K = 0.811\left(\frac{1+\cos\alpha}{16}\right)\left[\frac{2}{\pi}+\frac{\pi}{4}(1+\cos\alpha)+\frac{351.2\cos\alpha}{1+\cos\alpha}\left(\frac{R_a}{S_m}\right)\right]^{1/2}. \tag{21}$$

where S_m is mean spacing between roughness peaks. Kim et al. [80] also investigated CHF for water on superhydrophilic aluminum surfaces with contact angles of 7–16.3°, and reported that CHF increases from 165 W/cm^2 for $R_a = 0.11$ μm to 215 W/cm^2 for $R_a = 0.35$ μm, but has negligible dependence on surface roughness for $0.35 < R_a \leq 2.93$ μm.

3.2.4. Effects of pressure

When operating pressure is reduced considerably, pool boiling behavior is altered significantly due to the enormous increase in the vapor's specific volume [81]. Bewilogua et al. [51] and Kirichenko and Chernyakov [67] reported that dimensionless CHF given by Eq. (4) has a significant dependence on operating pressure. Katto et al. [82] found that CHF decreases with decreasing ratio of operating pressure to atmospheric pressure.

Deev et al. [83] used reduced pressure (ratio of operating to critical pressure), P/P_c, to assess the influence of pressure on pool boiling CHF. For $P/P_c \leq 0.75$, their CHF data for helium agreed well with the dimensionless form of Eq. (4) but required a higher value of $K = 0.2$ than that suggested by Kutateladze or Zuber. But, for $P/P_c > 0.75$, the Kutateladze-Zuber equation no longer applied, as the value for K varied considerably, a trend that Lyon et al. [84] later attributed to uncertainty in determination of physical properties at high pressures. Bailey et al. [77] noted that CHF has a power law dependence on saturation pressure. Labuntsov et al. [85] found experimentally that CHF for water and ethanol has a pressure dependence of $(P/P_c)^{0.15}$.

Using the least squares method, Bewilogua et al. [51] correlated CHF data for cryogenic liquids according to

$$\frac{q''_{CHF}}{q''_{CHF,max}} = 0.421 + 3.58\frac{P}{P_c} - 6.19\left(\frac{P}{P_c}\right)^2 + 2.21\left(\frac{P}{P_c}\right)^3, \tag{22}$$

where $q''_{CHF,max}$ is the peak value of CHF on a plot of CHF versus pressure. Shirai et al. [86] found that $q''_{CHF,max}$ for hydrogen occurs around $P = 0.3$ MPa. Dhir [87] reported that $q''_{CHF,max}$ according to Eq. (15) occurs around $P/P_c = 0.35$. Wang et al. [88] arrived at the same value of $P/P_c = 0.35$ for $q''_{CHF,max}$, and correlated CHF dependence on pressure by the relation

$$q''_{CHF} = \left[0.18 - 0.14(P/P_c)^{5.68}\right]\rho_g h_{fg}\left[\sigma g(\rho_f - \rho_g)/\rho_g^2\right]^{1/4}. \tag{23}$$

Inspired by Kutateladze's dimensional analysis, Soziev and Khrizolitova [89] developed a simple equation to predict CHF for very low pressures,

$$q''_{CHF} = 0.16\left\{1 + \left[\sigma g(\rho_f - \rho_g)\right]^{1/2}/P\right\}^{1/2}\rho_g h_{fg}\left[\sigma g(\rho_f - \rho_g)/\rho_g^2\right]^{1/4}. \tag{24}$$

Sakashita [90] noted that the Kutateladze-Zuber equation has the ability to predict CHF variations with pressure for ethanol and R-141b by adjusting the value of K in Eq. (4), but underestimates the pressure dependence for water. He explained these different trends by the fact that wettability of ethanol and R-141b is not affected by pressure, while wettability of water improves with increasing pressure. His water data agreed fairly well with predictions of Kirichenko and Chernyakov's [67] CHF correlation, which also accounted for wettability.

3.2.5. Effects of liquid viscosity

Borishanskii [91] proposed a modified CHF model to account for effects of liquid viscosity, but Moissis and Berenson [92] suggested that these effects are insignificant. Kim et al. [93] incorporated interfacial instability theory that accounts for viscosity effects into both Zuber's hydrodynamic model [20,31] and the macrolayer dryout model that will be discussed later. The modified instability analysis improved CHF predictions for water considerably, but improvements for organic fluids were quite small.

3.2.6. Summary of modified K for horizontal, upward-facing surface orientation

Table 1 summarizes, for the horizontal, upward-facing orientation, numerical values and/or empirical relations recommended by different investigators for dimensionless parameter K of the Kutateladze-Zuber equation. They include recommendations by Lienhard and Dhir [33,34], Chang [39], and Bailey et al. [77] consisting of different numerical values for K. They also include empirical relations by Watwe and Bar-Cohen [47] for effects of wall size and thermal properties, by Kirichenko and Chernyakov [67], Ramilison et al. [68], and Kim et al. [79] for contact angle, by Ramilison et al. [68] and Kim et al. [79] for surface roughness, by Wang et al. [88] and Soziev and Khrizolitova [89] for pressure, and by Borishanskii [91] for viscosity.

3.3. Modifications for other surface orientations

3.3.1. Effects of orientation

Yang et al. [94] found that a transition orientation angle exists for inclined surfaces beyond which CHF drops sharply, as shown in Fig. 5. They also reported that surface size has a strong influence on CHF for vertical and downward-facing orientations. They reported that the transition angle increases but CHF decreases with increasing surface size because of increased difficulty releasing the vapor. However, they did not recommend a correlation for transition angle as function of surface size or orientation angle. Gogonin

Table 1
Summary of dimensionless CHF for horizontal upward-facing surfaces based on the Kutateladze-Zuber equation.

Author(s)	Dimensionless CHF
Zuber [20,31]	$K = 0.131$
Lienhard and Dhir [33,34]	$K = 0.149$
Chang [39]	$K = 0.13$
Watwe and Bar-Cohen [47]	$K = \frac{\pi}{24}\left(\frac{S}{S+0.1}\right)\left\{1+\left(0.3014-0.01507L\sqrt{\frac{g(\rho_f-\rho_g)}{\sigma}}\right)\right\}\times\left\{1+0.03\left[\left(\frac{\rho_f}{\rho_g}\right)^{3/4}\frac{c_{pf}}{h_{fg}}\right]\Delta T_{sub}\right\}$
Kirichenko and Chernyakov [67]	$K = 0.171\,\frac{\left(1+0.324\times10^{-3}\alpha^2\right)^{1/4}}{(0.018\,\alpha)^{1/2}}$
Ramilison et al. [68]	$K = 0.0044\,(\pi-\alpha)^3 R_a^{0.125}$
Bailey et al. [77]	$K = 0.17$
Kim et al. [79]	$K = 0.811\,\left(\frac{1+\cos\alpha}{16}\right)\left[\frac{2}{\pi}+\frac{\pi}{4}(1+\cos\alpha)+\frac{351.2\cos\alpha}{1+\cos\alpha}\left(\frac{R_a}{S_m}\right)\right]^{1/2}$
Wang et al. [88]	$K = \left[0.18-0.14(P/P_c)^{5.68}\right]$
Soziev and Khrizolitova [89]	$K = 0.16\left\{1+\left[\sigma g(\rho_f-\rho_g)\right]^{1/2}/P\right\}^{1/2}$
Borishanskii [91]	$K = 0.13+4\left\{\frac{\rho_f\sigma^{3/2}}{\mu_f^2\left[g(\rho_f-\rho_g)\right]^{1/2}}\right\}^{-2/5}$

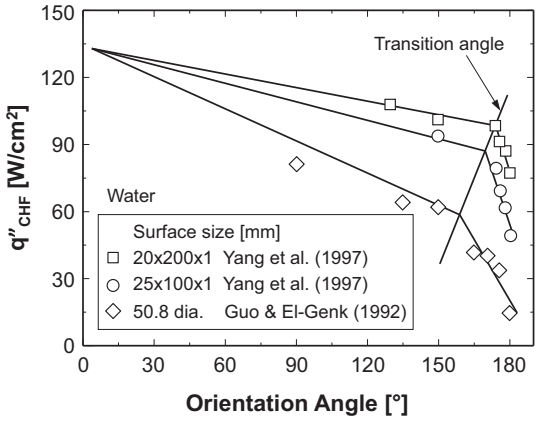

Fig. 5. Effects of heater size and orientation on pool boiling CHF. Adapted from Yang et al. [94].

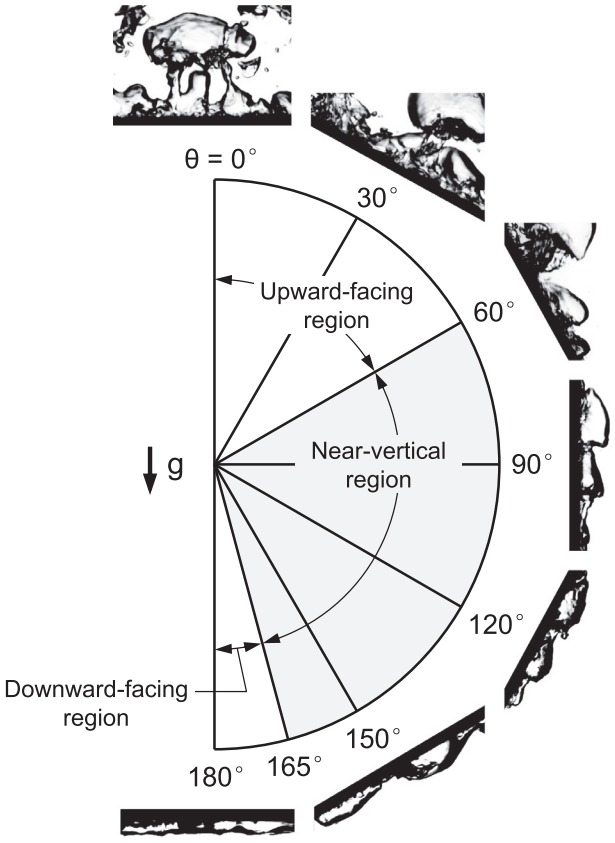

Fig. 6. Pool boiling photographs and regions of different CHF mechanisms for different surface orientations. Adapted from Howard and Mudawar [103].

and Kutateladze [95] reported similar trends of CHF versus surface size. Kim et al. [96] investigated CHF for pool boiling in inclined rectangular channels having different gaps between the surface and opposite cover plate, and measured transition angles of 165°, 170°, and 175° for 2, 5, and 10-mm gaps, respectively. However, they did not identify a transition angle for a 1-mm channel gap because of small surface width to length ratio for this gap.

Lyon [74], Priarone [97], El-Genk and Bostanci [98,99], Beduz et al. [100], and Brusstar et al. [101] all found that pool boiling CHF decreases slightly as surface orientation angle is increased from 0° to 90°, but decreases rapidly as orientation angle is increased towards 180° as vapor accumulation against the surface by buoyancy resists liquid access to the surface. Using a conductance probe to measure liquid-vapor content near the surface, Sakashita et al. [102] attributed the decrease in pool boiling CHF with increasing orientation angle to the lengthening of duration of passage of an upward-moving vapor mass.

Howard and Mudawar [103] conducted photographic studies at various surface orientations to determine CHF mechanism associated with each orientation range, and identified transition angles based on photographic analysis of near wall interfacial features. Shown in Fig. 6 are images captured just prior to CHF, which reveal that pool boiling CHF mechanisms can be divided into three regions with different vapor behaviors: (a) upward-facing region, $\theta = 0$–$60°$, where buoyancy serves to remove the vapor vertically off the surface, (b) near-vertical region, $\theta = 60$–$165°$, where a wavy liquid-vapor interface propagates along the surface, and (c) downward-facing region, $\theta > 165°$, corresponding to vapor stratification along surface and greatly reduced CHF. Because of the vast differences between observed vapor behaviors corresponding to the three regions, they indicated that it is impossible to account for orientation effects using a single CHF model, and proposed that three different models be developed for the three regions.

3.3.2. Summary of modified K for inclined surfaces

Despite many efforts to ascertain orientation effects on CHF, related theoretical modeling efforts are quite limited. In fact, most

available predictive tools for pool boiling CHF from inclined surfaces are empirical in nature, and consist of modifications to the original Kutateladze- Zuber equation. Also, to the best of the authors' knowledge, theoretical predictive tools for downward-facing surfaces are especially sparse, largely because of the stratified vapor rendering any optical access to the near-wall region quite difficult [104].

Vishnev [105] was the first to correlate the effects of surface orientation on pool boiling CHF for helium and water for different inclination angles, and for nitrogen, oxygen, hydrogen, neon, and Freon-14 for $\theta = 0°$, and his correlation remained widely popular. Other correlations with orientation angle include those by El-Genk and Bostanci [98] for HFE-7100, Arik and Bar-Cohen [106] for FC-72 and HFE-7100, and Chang and You [107] for FC-72. Kandlikar [69] and Liao et al. [70] addressed the combined effects of contact angle and orientation. El-Genk and Guo [108] developed fluid-dependent CHF correlations for $\theta = 90–180°$ using their own water data as well as nitrogen data of Beduz et al. [100] and helium data of Vishnev [105]. Another fluid-dependent correlation was developed by Priarone [97]. Brusstar and Merte [109,110] constructed an empirical correlation for subcooled pool boiling CHF based on a balance of buoyancy and drag forces parallel to the surface.

Table 2 summarizes the dimensionless pool boiling CHF correlations for inclined surfaces consisting of modifications to the original Kutateladze-Zuber equation.

4. Haramura and Katto macrolayer dryout model

4.1. Model rationale

Citing Gaertner's [111] visualization results for vapor structures in pool boiling, Katto and co-workers [82,112] related pool boiling CHF to intermittent behavior of coalescent vapor bubbles and consumption of a liquid macrolayer beneath the bubbles. Later, Haramura and Katto [21] refined the earlier model, describing the CHF mechanism, as shown in Fig. 7, as a large number of vapor stems emanating across the liquid macrolayer and cumulating in a large hovering bubble as a result of the Helmholtz instability, a behavior that was confirmed experimentally by Bang et al. [113]. They suggested that growth of the large bubble is the result of consumption of the macrolayer by evaporation, and that CHF is triggered when the liquid macrolayer dries out just before departure of the large bubble, which they expressed analytically as

$$q''_{CHF} = \rho_f h_{fg} \delta (1 - A_g/A_w) f, \tag{25}$$

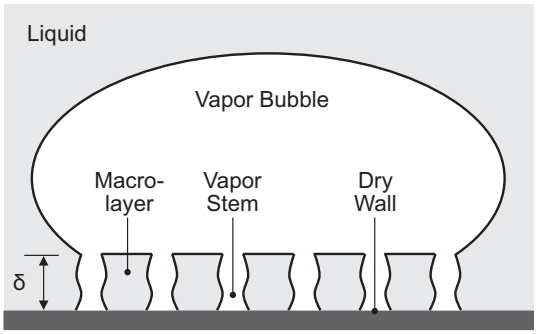

Fig. 7. Schematic of Haramura and Katto's macrolayer dryout CHF model.

where δ is the macrolayer thickness and f the bubble departure frequency. They further assumed that the macrolayer thickness lies between zero and half of the critical wavelength of Helmholtz instability, *i.e.*, $\delta = \lambda_H/4$, which resulted in the following expression for pool boiling CHF,

$$q''_{CHF} = 0.721 \left(\frac{A_g}{A_w}\right)^{5/8} \left(1 - \frac{A_g}{A_w}\right)^{5/16} \left[\left(\frac{\rho_f}{\rho_g} + 1\right) \Big/ \left(\frac{11}{16}\frac{\rho_f}{\rho_g} + 1\right)^{3/5}\right]^{5/16} \times \rho_g h_{fg} \left[\sigma(\rho_f - \rho_g) g / \rho_g^2\right]^{1/4}, \tag{26a}$$

or

$$\frac{q''_{CHF}}{q''_{CHF,Zuber}} = 5.5 \left(\frac{A_g}{A_w}\right)^{5/8} \left(1 - \frac{A_g}{A_w}\right)^{5/16} \left[\left(\frac{\rho_f}{\rho_g} + 1\right) \Big/ \left(\frac{11}{16}\frac{\rho_f}{\rho_g} + 1\right)^{3/5}\right]^{5/16}, \tag{26b}$$

where

$$\frac{A_g}{A_w} = 0.0584 \left(\frac{\rho_g}{\rho_f}\right)^{1/5}. \tag{27}$$

Sakashita and Kumada [114] used an interfacial depiction similar to that of Haramura and Katto [21] and constructed a CHF model for high pressures having the same form as the Kutateladze-Zuber equation.

Table 2
Summary of dimensionless CHF correlations for inclined surfaces.

Author(s)	Dimensionless CHF	Orientations
Kandlikar [69]	$K = \frac{1+\cos\alpha}{16}\left[\frac{2}{\pi} + \frac{\pi}{4}(1+\cos\alpha)\cos\theta\right]^{1/2}$	$\theta = 0–90°$
Liao et al. [70]	$K = 0.131\left[-0.73 + \frac{1.73}{1+10^{-0.021(185.4-\theta)}}\right]\left[1 + \frac{55-\alpha}{100}(0.56 - 0.0013\theta)\right]$	$\theta = 0–180°$
Priarone [97]	$K_{FC-72} = 0.165 f(\theta)$ $K_{HFE-7100} = 0.21 f(\theta)$ $f(\theta) = 1 - 0.001117\theta + 7.79401 \times 10^{-6}\theta^2 - 1.37678 \times 10^{-7}\theta^3$	$\theta = 0–175°$
El-Genk and Bostanci [98]	$K = \left[(0.229 - 4.27 \times 10^{-4}\theta)^{-6} + (0.577 - 2.98 \times 10^{-3}\theta)^{-6}\right]^{-1/6}$	$\theta = 0–180°$
Vishnev [105]	$K = 0.0125\,(190 - \theta)^{1/2}$	$\theta = 0–180°$
Arik and Bar-Cohen [106]	$K = 0.131\left(1 - 0.001117\theta + 7.79401 \times 10^{-6}\theta^2 - 1.37678 \times 10^{-7}\theta^3\right)$	$\theta = 0–180°$
Chang and You [107]	$q''_{CHF}/q''_{CHF,max} = 1 - 0.0012\theta\,\tan(0.414\theta) - 0.122\,\sin(0.318\theta)$	$\theta = 0–180°$
El-Genk and Guo [108]	$K_{water} = 0.034 + 0.0037(180 - \theta)^{0.656}$ $K_{nitrogen} = 0.033 + 0.0096(180 - \theta)^{0.479}$ $K_{helium} = 0.002 + 0.0051(180 - \theta)^{0.633}$	$\theta = 90–180°$
Brusstar and Merte [109,110]	$K = \frac{\pi}{24}\lvert\sin\theta\rvert^{1/2}\left[1 + 0.102\,(\frac{\rho_g}{\rho_f})^{1/4}\left(\frac{\rho_f\, c_{p,f}\Delta T_{sub}}{\rho_g h_{fg}}\right)\right]$	$\theta = 90–180°$

4.2. Alternative macrolayer thickness relations

Several investigators explored alternative methods for determining the thickness of the macrolayer used in the Haramura and Katto model. Rajvanshi et al. [115] suggested this thickness can be approximated by $\delta = \lambda_H/2$, yielding the relation

$$\delta = 0.0107\,\sigma\,\rho_g\left(1+\frac{\rho_g}{\rho_f}\right)\left(\frac{\rho_g}{\rho_f}\right)^{2/5}\left(\frac{h_{fg}}{q''}\right)^2, \tag{28a}$$

which is twice the thickness used by Haramura and Katto [21]. For $\rho_g/\rho_f \ll 1$, Rajvanshi et al. recommended simplifying Eq. (28a) to the form

$$\delta = 0.0107\,\sigma\,\rho_g\left(\frac{\rho_g}{\rho_f}\right)^{2/5}\left(\frac{h_{fg}}{q''}\right)^2, \tag{28b}$$

which agrees well with their measurements for water, methanol, ethanol, methyl ethyl ketone, isopropanol, and acetone.

Sadasivan et al. [116] argued that the Helmholtz instability is not an accurate basis for determining macrolayer thickness. Instead, they proposed a lateral bubble coalescence model, which they suggested is more accurate in describing the macrolayer formation. Later, Kumada and Sakashita [117] developed a semi-empirical relation for macrolayer thickness, also based on the lateral bubble coalescence mechanism,

$$\delta = 0.786\left[\frac{v_g^8\,\sigma^{11}}{\rho_f^6\,g^5(\rho_f-\rho_g)^5}\right]^{1/24}\left(\frac{\rho_g h_{fg}}{q''}\right)^{5/6}, \tag{29}$$

which agrees with their measurements for water, methanol, ethanol, and acetone. Sakashita and Ono [118] compared water CHF data with predictions of the macrolayer dryout model with different macrolayer thickness relations. As shown in Fig. 8, Eqs. (28b) and (29) by Rajvanshi et al. and Kumada and Sakashita, respectively, provide good predictions of the CHF data, as well as support the validity of the macrolayer dryout mechanism.

Chappidi et al. [119] developed a theoretical model for initial macrolayer thickness at CHF, which yielded the relation

$$\delta = \left[\frac{\rho_g}{\rho_f}\frac{A_g}{A_w}\left(1-\frac{A_g}{A_w}\right)^{-1}\sqrt{\frac{\rho_f+\rho_g}{\rho_f\rho_g}\sigma\,\tau}\right]^{2/3}, \tag{30}$$

where τ is the coalescent bubble hovering time. They also obtained the following empirical correlation between macrolayer thickness and mean vapor stem radius, R,

$$\delta = 1.1R. \tag{31}$$

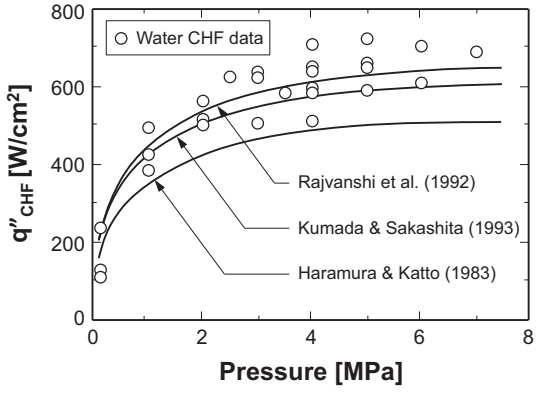

Fig. 8. Comparison of water CHF data with predictions of the macrolayer dryout model with different macrolayer thickness relations. Adapted from Sakashita and Ono [118].

Different formulations for macrolayer thickness are summarized in Table 3.

4.3. Modifications to macrolayer dryout model

Zhao et al. [120] argued that CHF is triggered by dryout of the microlayer under small bubbles rather than a macrolayer perforated by vapor stems. In other words, the large mushroom bubble above the liquid layer results from coalescence of small bubbles, a hypothesis supported by experiments by Nishio et al. [121] using the total reflection technique. Based on this concept, Zhao et al. derived a theoretical model of CHF, the simple form of which for water was expressed as

$$q''_{CHF} = 4.5\times10^4 d^{-0.44}, \tag{32}$$

where d is the diameter of individual bubbles before departure.

Using a small heated surface, Ahn and Kim [122] provided experimental evidence of the macrolayer at CHF. Their flow visualization experiments proved that lateral liquid inflow improves CHF compared to predictions of the hydrodynamic instability model of Zuber [20,31,32] and macrolayer dryout model of Haramura and Katto [21]. They proposed that CHF commences with macrolayer dryout along the outer perimeter of the surface, followed by merger of this outer dryout region with the central dry patch beneath the vapor mushroom.

Despite fairly good agreements between CHF data and predictions of the macrolayer dryout model, there remains uncertainty concerning the validity of the macrolayer dryout mechanism. For example, Xiao and Yu [123] reported that the macrolayer never dries out. Additionally, FC-72 experiments by Jung et al. [124] using high-speed infrared photography showed no evidence of regularly spaced vapor jets or a trapped liquid layer containing vapor stems that fed the hovering bubble overhead. Interestingly, these near-wall interfacial observations bring into question for the validity of both the hydrodynamic instability model and the macrolayer dryout model.

5. Hot/Dry spot model

5.1. Yagov model

The CHF model based on the hot/dry spot mechanism relates CHF to the presence of numerous small dry spots on the heater surface during nucleate boiling. This model was proposed by Yagov [125] in 1988 and modified to its latest version by Yagov [22] in 2014. Interestingly, several investigators have attempted to extrapolate CHF from nucleate boiling models [123,126–128]. As observed by Van Ouwerkerk [129], the trigger mechanism for CHF according to the hot/dry spot model is described as irreversible growth of a dry spot area on the surface as illustrated in Fig. 9.

Table 3
Summary of predictive formulations for macrolayer thickness.

Author(s)	Macrolayer thickness
Haramura and Katto [21]	$\delta = \frac{\lambda_H}{4} = 0.00536\,\sigma\,\rho_g\left(1+\frac{\rho_g}{\rho_f}\right)\left(\frac{\rho_g}{\rho_f}\right)^{2/5}\left(\frac{h_{fg}}{q''}\right)^2$
Rajvanshi et al. [115]	$\delta = \frac{\lambda_H}{2} = 0.0107\,\sigma\,\rho_g\left(1+\frac{\rho_g}{\rho_f}\right)\left(\frac{\rho_g}{\rho_f}\right)^{2/5}\left(\frac{h_{fg}}{q''}\right)^2$
Kumada and Sakashita [117]	$\delta = 0.786\left[\frac{v_g^8\,\sigma^{11}}{\rho_f^6\,g^5(\rho_f-\rho_g)^5}\right]^{1/24}\left(\frac{\rho_g h_{fg}}{q''}\right)^{5/6}$
Chappidi et al. [119]	$\delta = \left[\frac{\rho_g}{\rho_f}\frac{A_g}{A_w}\left(1-\frac{A_g}{A_w}\right)^{-1}\sqrt{\frac{\rho_f+\rho_g}{\rho_f\rho_g}\sigma\,\tau}\right]^{2/3}$

Based on this model, Yagov [22] proposed different CHF correlations for different ranges of reduced pressure. For low reduced pressures, $P/P_c < 0.001$,

$$q''_{CHF,l} = 0.5\,\frac{h_{fg}^{81/55}\,\sigma^{9/11}\,\rho_g^{13/110}\,k_f^{7/110}\,g^{21/55}\,f(Pr_f)}{\nu_f^{1/2}\,c_{p,f}^{3/10}\,R_i^{79/110}\,T_{sat}^{21/22}}, \tag{33}$$

where R_i is the individual gas constant, and the Prandtl number function $f(Pr_f)$ is expressed as

$$f(Pr_f) = \left(\frac{Pr_f^{9/8}}{1 + 2Pr_f^{1/4} + 0.6Pr_f^{19/24}}\right)^{4/11}. \tag{34}$$

For high reduced pressures, $P/P_c > 0.03$,

$$q''_{CHF,h} = 0.06\,h_{fg}\,\rho_g^{3/5}\sigma^{2/5}[g(\rho_f - \rho_g)/\mu_f]^{1/5}. \tag{35}$$

Yagov also recommended the following weighting function to determine CHF for intermediate reduced pressures, $0.001 \le P/P_c \le 0.03$,

$$q''_{CHF} = \left(q''^3_{CHF,h} + q''^3_{CHF,l}\right)^{1/3}. \tag{36}$$

Notice that, unlike the hydrodynamic instability model, the dry spot model shows a dependence on liquid viscosity. These viscosity effects are more appreciable for lower pressures, Eqs. (33) and (34), and much weaker for high pressures, Eq. (35). Yagov reported that CHF values predicted by Eq. (35) are close to those of hydrodynamic instability models because most available experimental data are within moderate and high reduced pressures for which viscosity effects are quite weak.

5.2. Theofanous and Dinh formulation

Theofanous et al. [23,130] observed temperature patterns on the surface during nucleate boiling using a high-speed, high-resolution infrared camera. They detected lower temperatures in cold spots, identified as active nucleation sites, because of effective heat removal under the growing bubbles. As the heat flux is increased, the pattern of cold spots becomes more and more regular, although the pool's two-phase motion becomes more chaotic. Further increases in heat flux cause hot spots to develop within originally cold spots, and CHF is triggered by irreversible growth of hot spots, as depicted in Fig. 10. Similarly, Jung et al. [124] proposed that CHF occurs as dry spot size increases faster than the increase in heat transfer through the wetted area, indicating that higher CHF can be achieved by either increasing wetted fraction of the surface or improving heat transfer through the wetted portions.

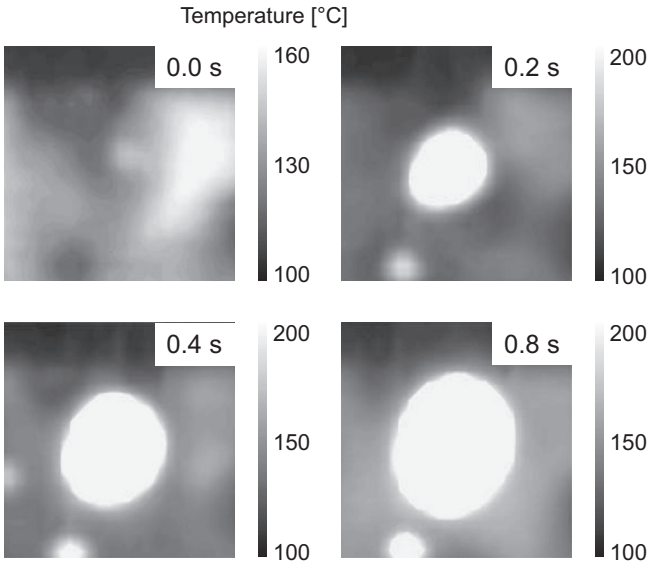

Fig. 10. Photographs of dry-spot growth at CHF for water. Adapted from Theofanous et al. [23].

By assuming that CHF is governed by dynamics and instability of the liquid microlayer, a follow-up study by Theofanous and Dinh [131] culminated in a CHF relation similar to the Kutateladze-Zuber equation,

$$q''_{CHF} = k^{-1/2}\rho_g h_{fg}\left[\sigma g(\rho_f - \rho_g)/\rho_g^2\right]^{1/4}, \tag{37}$$

where k is a function of surface conditions, decreasing with increasing surface wettability. However, they did not recommend a method for calculating this parameter. Later, Kim et al. [59] derived a theoretical relation for k using Lord Rayleigh's formula for volume of static liquid meniscus [132],

$$k = \left(1 - \frac{\sin\alpha}{2} - \frac{\pi/2 - \alpha}{2\cos\alpha}\right)^{-1/2}, \tag{38}$$

which is applicable to hydrophilic surfaces, *i.e.,* with contact angles below 90°.

5.3. Other observations of dry spot behavior

Recently, using the total reflection technique, Chu et al. [133] showed that, contrary to common belief that a thin, stable liquid film resides beneath large coalescent hovering bubbles, the base

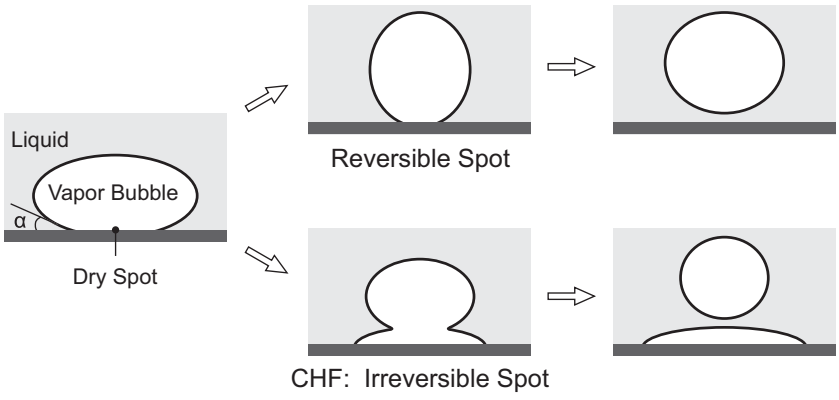

Fig. 9. Schematic of CHF model based on irreversible dry spot hypothesis.

of these bubbles is almost dry even before CHF initiation. Choi et al. [134] proposed hydraulic and thermal criteria for the onset of irreversible dry spots. The hydraulic criterion states that the irreversible condition will occur when the number of dry spots reaches a critical level where the spots begin to contact one another. The thermal criterion attributes the irreversible condition to the peripheral temperature of dry spots reaching the Leidenfrost temperature, which prevents surface rewetting even after the bubble detachment. Choi et al. suggested that CHF would occur once both criteria are fulfilled. However, Kim et al. [135] found that the surface temperature initiating the formation of irreversible dry spots in water is 134 °C, far lower than the Leidenfrost temperature and maximum liquid-contact temperature. Both Kim et al. and Chu et al. [136] observed that formation of an irreversible dry spot results from vigorous bubble nucleation near the triple-phase contact line, which inhibits wetting of the dry spot.

It is expected that development of more powerful flow visualization and measurement techniques will greatly benefit the understanding of interfacial behavior near the dry spot, and help improve the predictive capabilities of CHF models based on the dry spot mechanism.

6. Galloway and Mudawar interfacial lift-off model

6.1. Vertical and near-vertical orientations

Based on extensive high-speed video motion analysis, Galloway and Mudawar [137] postulated that CHF in flow boiling will occur when vapor momentum becomes strong enough to lift the bulk liquid away from the surface, a mechanism they used to construct the theoretical *interfacial lift-off model* [138] for CHF in flow boiling. Later, Mudawar and co-workers [24,103] found that the interfacial behavior at CHF in pool boiling along a vertical surface bears close resemblance to flow boiling CHF. Using pool boiling images such as those in Fig. 11(a), they proposed a series of events that culminate in CHF. At heat fluxes slightly below CHF, intense vapor production results in a vapor layer that propagates along the surface. Helmholtz instability produces pronounced waves in this layer, permitting liquid contact with the surface only in 'wetting fronts' corresponding to the wave troughs. These wetting fronts sweep along the surface, providing the last source of cooling for the surface. CHF is described to result from loss of wetting fronts when intense vapor momentum perpendicular to the surface just exceeds the opposing pressure force resulting from interfacial curvature,

$$\rho_g\left[\frac{q''_l}{\rho_g h_{fg}(1+c_{p,f}\Delta T_{sub}/h_{fg})}\right]^2 = \overline{P_f - P_g}, \tag{39}$$

where q''_l is the localized heat flux in the wetting front. Mudawar et al. [24] showed that the average pressure difference resulting from interfacial curvature can be expressed as

$$\overline{P_f - P_g} = 2\sqrt{2}\pi\frac{\sigma\delta}{\lambda_c^2}, \tag{40}$$

where δ is the mean vapor layer thickness, and λ_c the critical wavelength corresponding to the onset of Helmholtz instability. Substituting Eq. (40) into Eq. (39) and assuming that wetting front span is one-fourth the critical wavelength (*i.e.*, $q''_{CHF} = q''_l/4$) yield

$$q''_{CHF} = \frac{1}{4}\rho_g h_{fg}\left(1+\frac{c_{p,f}\Delta T_{sub}}{h_{fg}}\right)\left[\left(2\sqrt{2}\pi\right)\frac{\sigma\delta}{\rho_g\lambda_c^2}\right]^{1/2}. \tag{41}$$

In this model, analytical expressions for δ and λ_c are obtained from a separated flow model, which yields

$$\delta = \frac{q''_{CHF}}{\rho_g h_{fg}\left(1+\frac{c_{p,f}\Delta T_{sub}}{h_{fg}}\right)}\left\{g\left(\frac{\rho_f-\rho_g}{\rho_g}\right)\frac{q''_{CHF}}{0.5 f_i \rho_g h_{fg}\left(1+\frac{c_{p,f}\Delta T_{sub}}{h_{fg}}\right)}\right\}^{-1/3}\lambda_c^{2/3} \tag{42a}$$

and

$$\lambda_c = \left[2\pi\sigma\left(\frac{\rho_f+\rho_g}{\rho_f\rho_g}\right)\right]^{3/5}\left\{g\left(\frac{\rho_f-\rho_g}{\rho_g}\right)\frac{q''_{CHF}}{0.5 f_i \rho_g h_{fg}\left(1+\frac{c_{p,f}\Delta T_{sub}}{h_{fg}}\right)}\right\}^{-2/5}, \tag{42b}$$

where f_i is interfacial friction factor equal to 0.5. Substituting Eqs. (42a) and (42b) into Eq. (41) yields

$$q''_{CHF} = 2^{-113/24}3^{5/6}\left(\frac{\pi}{f_i}\right)^{1/4}\left(\frac{\rho_f}{\rho_f+\rho_g}\right)\rho_g h_{fg}\left(1+\frac{c_{p,f}\Delta T_{sub}}{h_{fg}}\right)\left[\frac{\sigma g(\rho_f-\rho_g)}{\rho_g^2}\right]^{1/4}, \tag{43}$$

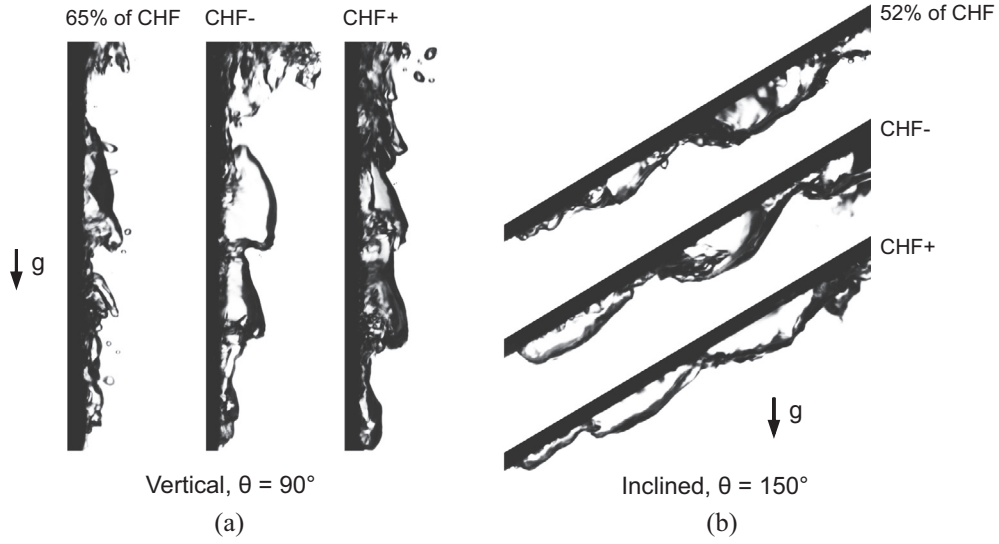

Fig. 11. Pool boiling images for increasing heat flux at surface orientations of (a) $\theta = 90°$ and (b) $\theta = 150°$. Adapted from Howard and Mudawar [103].

which can be further simplified for saturated conditions and pressures excluding near-critical to

$$q''_{CHF} = 0.151\,\rho_g h_{fg}\left[\sigma g(\rho_f - \rho_g)\Big/\rho_g^2\right]^{1/4}, \tag{44}$$

which is identical in form to the Kutateladze-Zuber equation. Notice that the presence of the gravity term in Eq. (44) results from the buoyancy driven vapor flow, rather than the Taylor instability in Zuber's model [20,31].

Follow-up study by Howard and Mudawar [103] found that the interfacial lift-off trigger mechanism of CHF is not limited to the vertical orientation, but includes all near-vertical orientations in the range of $\theta = 60$–$165°$ as depicted in Fig. 11(b) and shown schematically in Fig. 12. The same model was effective in predicting the transition angle of 165° between the near-vertical and downward-facing regions shown earlier in Fig. 6. Using data from a number of sources, Howard and Mudawar also showed that orientation effects on CHF for $0 < \theta < 90°$ are very weak, meaning Eq. (44) is equally valid for $\theta = 0°$ and 90°. The interfacial lift-off model is supported by recent observations of pool boiling CHF for different orientations by Kim et al. [96] and Zhong et al. [139].

Interestingly, the interfacial lift-off model has shown great versatility and accuracy in predicting flow boiling CHF in a variety of situations, including microgravity [140,141]. This is especially important in that it validates the CHF dependence on gravity. Overall, better success has been achieved in predicting reduced gravity CHF for flow boiling than for pool boiling [142].

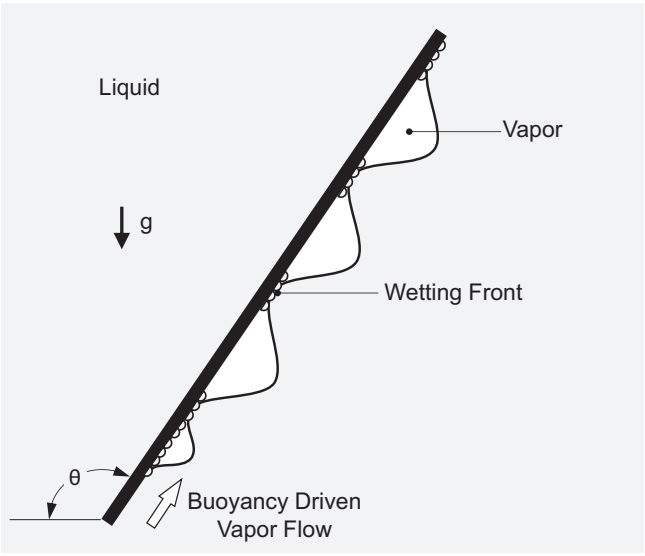

Fig. 12. Schematic of interfacial lift-off CHF model for pool boiling on a near-vertical surface. Adapted from Howard and Mudawar [103].

6.2. Horizontal, upward-facing orientation

Guan et al. [104] observed the interfacial lift-off process in pool boiling CHF for the upward-facing orientation as well. Fig. 13 provides a sequence of images that capture the lift-off process for pentane. At $t = 0$ s, a small vapor patch is observed at the right edge of the surface propagating from right to left until $t = 2.8$ s, when the entire surface becomes blanketed with vapor. According to their observations, Guan et al. introduced a CHF model for pool boiling based on the mechanism of liquid macrolayer lift-off, which is based on the interfacial lift-off model of Galloway and Mudawar [138]. A key difference from the original model is that the Guan et al. model, which is depicted schematically in Fig. 14, does not require a separated flow model to determine the vapor layer parameters. Instead, it uses momentum conservation and Laplace condition for the vapor-liquid interface to derive an expression for upward vapor velocity corresponding to CHF,

$$u_g = \sqrt{\frac{2\sigma}{r\rho_g}}, \tag{45}$$

where r is the local radius of curvature of the interface. The vapor velocity is highest when the local radius is minimum, expressed as

$$r = \sqrt{\frac{\lambda_d^2}{2\pi^2\delta}}, \tag{46}$$

where δ is the liquid macrolayer thickness, which is predicted according to the theoretical formulation of Rajvanshi et al. [115]. This approach culminates in the following expression for pool boiling CHF,

$$q''_{CHF} = \rho_g u_g h_{fg} = 0.2445\left(1+\frac{\rho_g}{\rho_f}\right)^{1/4}\left(\frac{\rho_g}{\rho_f}\right)^{1/10}\rho_g h_{fg}\left[\frac{\sigma g(\rho_f-\rho_g)}{\rho_g^2}\right]^{1/4}, \tag{47}$$

which bears some resemblance to the Kutateladze-Zuber equation.

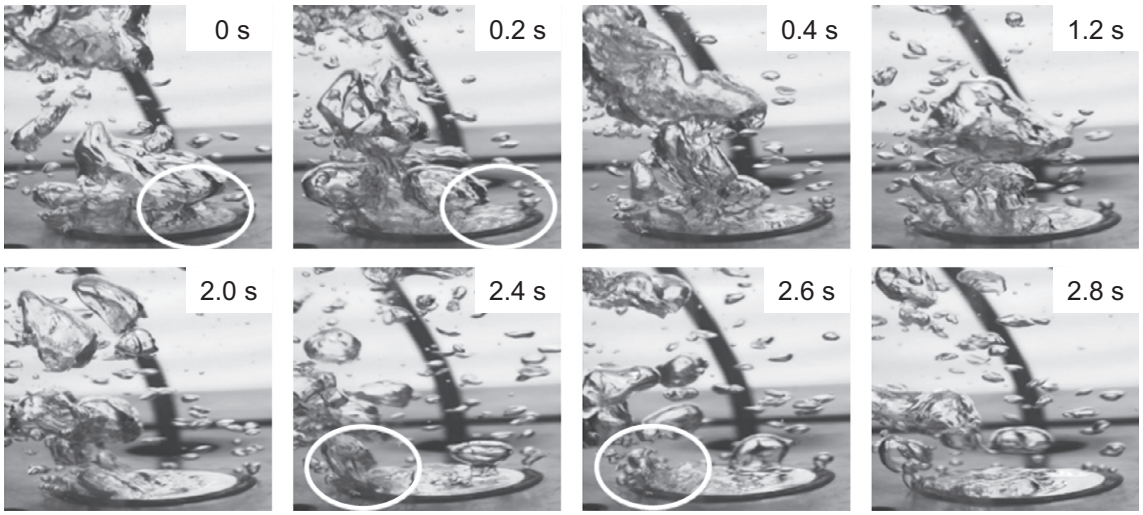

Fig. 13. Images of interfacial lift-off in pool boiling for pentane at $\Delta T_{sat} = 20$ °C and $P_g = 150$ kPa. Adapted from Guan et al. [104].

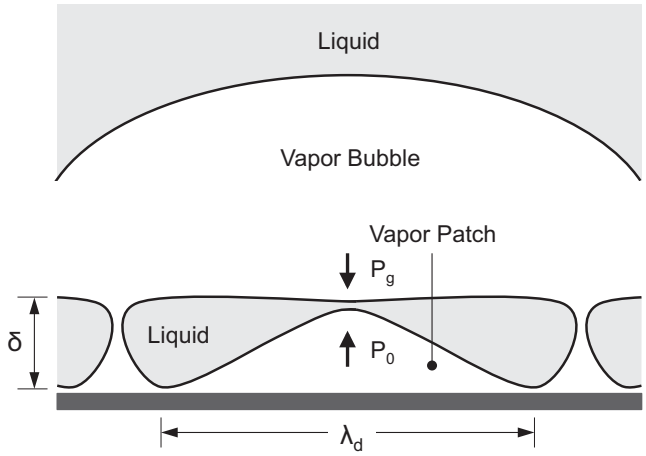

Fig. 14. Schematic of macrolayer lift-off during pool boiling CHF from a horizontal upward-facing surface. Adapted from Guan et al. [104].

Overall, the interfacial lift-off mechanism for pool boiling CHF is based on microscopic observations and features theoretical appeal not found with empirical CHF correlations. Additionally, because of reliance on hydrodynamic instability theory, it leads to a dimensionless formulation similar to those of the Kutateladze-Zuber equation.

7. Concluding remarks

This paper is the first part of a two-part study on pool boiling critical heat flux (CHF) from flat surfaces. The primary objective of this part is to review published CHF models, including CHF trigger mechanisms and parametric influences. Key observations from the study can be summarized as follows:

(1) Aside from Kutateladze's 1948 pioneering CHF formulation, which is based on dimensional analysis, five different CHF mechanisms are prevalent in the literature: bubble interference, hydrodynamic instability, macrolayer dryout, hot/dry spot, and interfacial lift-off. Among the five mechanisms, Zuber's hydrodynamic instability theory has received the most attention because of both its mechanistic formulation and theoretical appeal. More recently, the interfacial lift-off mechanism, which is also theoretically based, has received significant experimental validation, and offers the advantage of tackling different surface orientations.

(2) The heat transfer literature includes numerous investigations into influences of important parameters on CHF, including pressure, surface size and roughness, surface orientation, and contact angle. Studies also reveal that CHF increases with increasing wall thickness but reaches asymptotic value above a thickness threshold. Therefore, it is essential to rely on data for wall thicknesses that exceed this threshold. Overall, there is a shortage of data with broad coverage of all relevant parameters and for fluids with vastly different thermal properties. There is also severe shortage of data for the horizontal, downward-facing surface orientation. These facts point to a need for more strategically planned future experiments that would also include microphotographic analysis of near-wall interfacial features, in order to validate or dispute proposed CHF mechanisms.

(3) Given the complexity of the CHF phenomenon and dependence on a variety of parameters, it is crucial that available data be amassed into a single consolidated database for assessment of different models and correlations. In the future, this database would continue to grow as new data are acquired to cover major gaps in the coverage of relevant parameters. Developing this consolidated database is a key objective of the second part of this study.

Conflict of interest

None declared.

Acknowledgement

Support of the National Natural Science Foundation of China under Grant No. 51506023 and the Fundamental Research Funds for Central Universities of Ministry of Education of China under Grant No. DUT17RC(4)22 is gratefully acknowledged.

Appendix A. Supplementary material

Supplementary data associated with this article can be found, in the online version, at https://doi.org/10.1016/j.ijheatmasstransfer.2017.09.134.

References

[1] I. Mudawar, Assessment of high-heat-flux thermal management schemes, IEEE Trans. Compon. Packag. Technol. 24 (2001) 122–141.
[2] I. Mudawar, Recent advances in high-flux, two-phase thermal management, J. Therm. Sci. Eng. Appl. 5 (2013) 021012.
[3] T.J. LaClair, I. Mudawar, Thermal transients in a capillary evaporator prior to the initiation of boiling, Int. J. Heat Mass Transfer 43 (2000) 3937–3952.
[4] I. Mudawar, T.M. Anderson, Optimization of enhanced surfaces for high flux chip cooling by pool boiling, J. Electron. Packag. 115 (1993) 89–100.
[5] J.A. Shmerler, I. Mudawwar, Local heat transfer coefficient in wavy free-falling turbulent liquid films undergoing uniform sensible heating, Int. J. Heat Mass Transfer 31 (1988) 67–77.
[6] C.O. Gersey, I. Mudawar, Effects of heater length and orientation on the trigger mechanism for near-saturated flow boiling critical heat flux–I. Photographic study and statistical characterization of the near-wall interfacial features, Int. J. Heat Mass Transfer 38 (1995) 629–641.
[7] T.C. Willingham, I. Mudawar, Forced-convection boiling and critical heat flux from a linear array of discrete heat sources, Int. J. Heat Mass Transfer 35 (1992) 2879–2890.
[8] D.E. Maddox, I. Mudawar, Single-and two-phase convective heat transfer from smooth and enhanced microelectronic heat sources in a rectangular channel, J. Heat Transfer 101 (1989) 1045–1052.
[9] J. Lee, I. Mudawar, Critical heat flux for subcooled flow boiling in micro-channel heat sinks, Int. J. Heat Mass Transfer 52 (2009) 3341–3352.
[10] J. Lee, I. Mudawar, Fluid flow and heat transfer characteristics of low temperature two-phase micro-channel heat sinks–part 1: experimental methods and flow visualization results, Int. J. Heat Mass Transfer 51 (2008) 4315–4326.
[11] D.D. Hall, I. Mudawar, Ultra-high critical heat flux (CHF) for subcooled water flow boiling–II: high-CHF database and design equations, Int. J. Heat Mass Transfer 42 (1999) 1429–1456.
[12] S. Mukherjee, I. Mudawar, Pumpless loop for narrow channel and micro-channel boiling, J. Electron. Packag. 125 (2003) 431–441.
[13] D.C. Wadsworth, I. Mudawar, Enhancement of single-phase heat transfer and critical heat flux from an ultra-high-flux simulated microelectronic heat source to a rectangular impinging jet of dielectric liquid, J. Heat Transfer 114 (1992) 764–768.
[14] J.D. Bernardin, I. Mudawar, A Leidenfrost point model for impinging droplets and sprays, J. Heat Transfer 126 (2004) 272–278.
[15] M. Visaria, I. Mudawar, Effects of high subcooling on two-phase spray cooling and critical heat flux, Int. J. Heat Mass Transfer 51 (2008) 5269–5278.
[16] M.K. Sung, I. Mudawar, Experimental and numerical investigation of single-phase heat transfer using a hybrid jet-impingement/micro-channel cooling scheme, Int. J. Heat Mass Transfer 49 (2006) 682–694.
[17] G. Liang, I. Mudawar, Review of spray cooling–part 1: single-phase and nucleate boiling regimes, and critical heat flux, Int. J. Heat Mass Transfer 115 (2017) 1174–1205.
[18] G. Liang, I. Mudawar, Review of spray cooling–part 2: high temperature boiling regimes and quenching applications, Int. J. Heat Mass Transfer 115 (2017) 1206–1222.
[19] W.M. Rohsenow, P. Griffith, Correlation of maximum heat transfer data for boiling of saturated liquids, Chem. Eng. Prog. Symp. Ser. 52 (1955) 47–49.
[20] N. Zuber, On the stability of boiling heat transfer, Trans. ASME 80 (1958) 711–720.

[21] Y. Haramura, Y. Katto, A new hydrodynamic model of critical heat flux, applicable widely to both pool and forced convection boiling on submerged bodies in saturated liquids, Int. J. Heat Mass Transfer 26 (1983) 389–399.
[22] V.V. Yagov, Is a crisis in pool boiling actually a hydrodynamic phenomenon?, Int J. Heat Mass Transfer 73 (2014) 265–273.
[23] T.G. Theofanous, T.-N. Dinh, J.P. Tu, A.T. Dinh, The boiling crisis phenomenon: Part II: dryout dynamics and burnout, Exp. Thermal Fluid Sci. 26 (2002) 793–810.
[24] I. Mudawar, A.H. Howard, C.O. Gersey, An analytical model for near-saturated pool boiling critical heat flux on vertical surfaces, Int. J. Heat Mass Transfer 40 (1997) 2327–2339.
[25] S.S. Kutateladze, On the transition to film boiling under natural convection, Kotloturbostroenie 3 (1948) 10–12.
[26] S.S. Kutateladze, Boiling and bubbling heat transfer under free convection of liquid, Int. J. Heat Mass Transfer 22 (1979) 281–299.
[27] S.S. Kutateladze, Boiling heat transfer, Int. J. Heat Mass Transfer 4 (1961) 31–45.
[28] G. Liang, I. Mudawar, Pool boiling critical heat flux (CHF)–part 2: assessment of models and correlations, Int. J. Heat Mass Transfer (2017), https://doi.org/10.1016/j.ijheatmasstransfer.2017.09.073 (in press).
[29] M. Arik, A. Kosar, H. Bostanci, A. Bar-Cohen, Pool boiling critical heat flux in dielectric liquids and nanofluids, in: Y.I. Cho, G.A. Greene (Eds.), Advances in Heat Transfer, vol. 43, 2011, pp. 1–76.
[30] Y. Chang, N.W. Snyder, Heat transfer in saturated boiling, Chem. Eng. Prog. Symp. Ser. 56 (1960) 25–28.
[31] N. Zuber, Hydrodynamic aspects of boiling heat transfer (PhD Dissertation), University of California, Los Angeles, USA, 1959.
[32] N. Zuber, M. Tribus, J.W. Westwater, The hydrodynamic crisis in pool boiling of saturated and subcooled liquids, in: International Developments in Heat Transfer: Proceedings of the Int. Heat Transfer Conference, Boulder, USA, 1961, pp. 230–236.
[33] J.H. Lienhard, V.K. Dhir, Extended Hydrodynamic Theory of the Peak and Minimum Pool Boiling Heat Fluxes, NASA Report No. CR-2270, University of Kentucky, Lexington, 1973.
[34] J.H. Lienhard, V.K. Dhir, Hydrodynamic prediction of peak pool-boiling heat fluxes from finite bodies, J. Heat Transfer 95 (1973) 152–158.
[35] J.H. Lienhard, V.K. Dhir, D.M. Riherd, Peak pool boiling heat-flux measurements on finite horizontal flat plates, J. Heat Transfer 95 (1973) 477–482.
[36] M.-C. Lu, C.-H. Huang, C.-T. Huang, Y.-C. Chen, A modified hydrodynamic model for pool boiling CHF considering the effects of heater size and nucleation site density, Int. J. Therm. Sci. 91 (2015) 133–141.
[37] M. Pezo, V. Stevanovic, Numerical prediction of critical heat flux in pool boiling with the two-fluid model, Int. J. Heat Mass Transfer 54 (2011) 3296–3303.
[38] C. Zhang, P. Cheng, F. Hong, Mesoscale simulation of heater size and subcooling effects on pool boiling under controlled wall heat flux conditions, Int. J. Heat Mass Transfer 101 (2016) 1331–1342.
[39] Y.-P. Chang, An analysis of the critical conditions and burnout in boiling heat transfer, Report No. TID-14004, University of Notre Dame, Notre Dame, 1961.
[40] F. Tachibana, M. Akiyama, H. Kawamura, Non-hydrodynamic aspects of pool boiling burnout, J. Nucl. Sci. Technol. 4 (1967) 121–130.
[41] I. Golobič, A.E. Bergles, Effects of heater-side factors on the saturated pool boiling critical heat flux, Exp. Therm. Fluid Sci. 15 (1997) 43–51.
[42] K. Ferjančič, I. Golobič, Surface effects on pool boiling CHF, Exp. Therm. Fluid Sci. 25 (2002) 565–571.
[43] I.I. Gogonin, Influence of the thickness of a wall and of its thermophysical characteristics on the critical heat flux in boiling, J. Eng. Phys. Thermophys. 82 (2009) 1175–1183.
[44] V.A. Grigoriev, V.V. Klimenko, Y.M. Pavlov, Y.V. Amitestov, The influence of some heating surface properties on the CHF in cryogenics liquids boiling, in: Proceedings of the 6th International Heat Transfer Conference, Toronto, Canada, 1978.
[45] I.I. Gogonin, Dependence of the critical heat flux at boiling on the coolant physical properties, Thermophys. Aeromech. 16 (2009) 111–118.
[46] A. Bar-Cohen, A. McNeil, Parametric effects on pool boiling critical heat flux in highly wetting liquids, in: Proceedings of the Engineering Foundation Conference on Pool and External Flow Boiling, Santa Barbara, USA, 1992, pp. 171–176.
[47] A.A. Watwe, A. Bar-Cohen, Modeling of conduction effects on pool boiling CHF of dielectric liquids, in: Proceedings of the 32nd National Heat Transfer Conference, Baltimore, USA, 1997.
[48] M. Arik, A. Bar-Cohen, Effusivity-based correlation of surface property effects in pool boiling CHF of dielectric liquids, Int. J. Heat Mass Transfer 46 (2003) 3755–3764.
[49] C. Bombardieri, C. Manfletti, Influence of wall material on nucleate pool boiling of liquid nitrogen, Int. J. Heat Mass Transfer 94 (2016) 1–8.
[50] M. Jergel, R. Stevenson, Heat transfer to boiling helium from aluminium surfaces, Cryogenics 12 (1972) 312–313.
[51] L. Bewilogua, R. Knöner, H. Vinzelberg, Heat transfer in cryogenic liquids under pressure, Cryogenics 15 (1975) 121–125.
[52] B.J. Stock, Observations on Transition Boiling Heat Transfer Phenomena, Report No. ANL-6175, Argonne National Laboratory, Argonne, USA, 1960.
[53] H. O'Hanley, C. Coyle, J. Buongiorno, T. McKrell, L.-W. Hu, M. Rubner, R. Cohen, Separate effects of surface roughness, wettability, and porosity on the boiling critical heat flux, Appl. Phys. Lett. 103 (2013) 024102.
[54] R.F. Gaertner, Effect of Heater Surface Chemistry on the Level of Burnout Heat Flux in Pool Boiling, Report No. 63-RL-3449C, General Electric Research Laboratory, Schenectady, USA, 1963.
[55] C.P. Costello, W.J. Frea, A salient nonhydrodynamic effect on pool boiling burnout of small semicylindrical heaters, AIChE Chem. Eng. Progr. Symp. Ser. 61 (1963) 258–268.
[56] M. Maracy, R.H.S. Winterton, Hysteresis and contact angle effects in transition pool boiling of water, Int. J. Heat Mass Transfer 31 (1988) 1443–1449.
[57] E. Hahne, T. Diesselhorst, Hydrodynamic and surface effects on the peak heat flux in pool boiling, in: Proceedings of the 6th International Heat Transfer Conference, Toronto, Canada, 1978, pp. 209–214.
[58] E. Forrest, E. Williamson, J. Buongiorno, L.-W. Hu, M. Rubner, R. Cohen, Augmentation of nucleate boiling heat transfer and critical heat flux using nanoparticle thin-film coatings, Int. J. Heat Mass Transfer 53 (2010) 58–67.
[59] S.J. Kim, I.C. Bang, J. Buongiorno, L.W. Hu, Surface wettability change during pool boiling of nanofluids and its effect on critical heat flux, Int. J. Heat Mass Transfer 50 (2007) 4105–4116.
[60] A.R. Neto, J.L.G. Oliveira, J.C. Passos, Heat transfer coefficient and critical heat flux during nucleate pool boiling of water in the presence of nanoparticles of alumina, maghemite and CNTs, Appl. Therm. Eng. 111 (2017) 1493–1506.
[61] J.M. Kim, D.I. Yu, H.S. Park, K. Moriyama, M.H. Kim, Smart surface in pool boiling: thermally-induced wetting transition, Int. J. Heat Mass Transfer 109 (2017) 231–241.
[62] S. Mori, Y. Utaka, Critical heat flux enhancement by surface modification in a saturated pool boiling: a review, Int. J. Heat Mass Transfer 108 (2017) 2534–2557.
[63] D. Ciloglu, A. Bolukbasi, A comprehensive review on pool boiling of nanofluids, Appl. Therm. Eng. 84 (2015) 45–63.
[64] X. Fang, Y. Chen, H. Zhang, W. Chen, A. Dong, R. Wang, Heat transfer and critical heat flux of nanofluid boiling: a comprehensive review, Renewable Sustainable Energy Rev. 62 (2016) 924–940.
[65] B. Truong, L.-W. Hu, J. Buongiorno, T. McKrell, Modification of sandblasted plate heaters using nanofluids to enhance pool boiling critical heat flux, Int. J. Heat Mass Transfer 53 (2010) 85–94.
[66] S.P. Liaw, V.K. Dhir, Effect of surface wettability on transition boiling heat transfer from a vertical surface, in: Proceedings of the 8th International Heat Transfer Conference, San Francisco, USA, 1986, pp. 2031–2036.
[67] Y.A. Kirichenko, P.S. Chernyakov, Determination of the first critical thermal flux on flat heaters, J. Eng. Phys. Thermophys. 20 (1971) 699–703.
[68] J.M. Ramilison, P. Sadasivan, J.H. Lienhard, Surface factors influencing burnout on flat heaters, J. Heat Transfer 114 (1992) 287–290.
[69] S.G. Kandlikar, A theoretical model to predict pool boiling CHF incorporating effects of contact angle and orientation, J. Heat Transfer 123 (2001) 1071–1079.
[70] L. Liao, R. Bao, Z. Liu, Compositive effects of orientation and contact angle on critical heat flux in pool boiling of water, Heat Mass Transfer 44 (2008) 1447–1453.
[71] H.T. Phan, R. Bertossi, N. Caney, P. Marty, S. Colasson, A model to predict the effect of surface wettability on critical heat flux, Int. Commun. Heat Mass Transfer 39 (2012) 1500–1504.
[72] G. Liang, I. Mudawar, Review of drop impact on heated walls, Int. J. Heat Mass Transfer 106 (2017) 103–126.
[73] P.J. Berenson, Experiments on pool-boiling heat transfer, Int. J. Heat Mass Transfer 5 (1962) 985–999.
[74] D.N. Lyon, Peak nucleate-boiling heat fluxes and nucleate-boiling heat-transfer coefficients for liquid N_2, liquid O_2 and their mixtures in pool boiling at atmospheric pressure, Int. J. Heat Mass Transfer 7 (1964) 1097–1116.
[75] J.M. Ramilison, J.H. Lienhard, Transition boiling heat transfer and the film transition regime, J. Heat Transfer 109 (1987) 746–752.
[76] S. Nishio, G.R. Chandratilleke, Steady-state pool boiling heat transfer to saturated liquid helium at atmospheric pressure, JSME Int. J. Ser. II 32 (1989) 639–645.
[77] W. Bailey, E. Young, C. Beduz, Y. Yang, Pool boiling study on candidature of pentane, methanol and water for near room temperature cooling, in: Thermal and Thermomechanical Phenomena in Electronics Systems, IEEE, San Diego, USA, 2006, pp. 599–603.
[78] C.-K. Guan, B. Bon, J. Klausner, R. Mei, Comparison of CHF enhancement on microstructured surfaces with a predictive model, Heat Transfer Eng. 35 (2014) 452–460.
[79] J. Kim, S. Jun, R. Laksnarain, S.M. You, Effect of surface roughness on pool boiling heat transfer at a heated surface having moderate wettability, Int. J. Heat Mass Transfer 101 (2016) 992–1002.
[80] J. Kim, S. Jun, S.M. You, Effect of surface roughness on pool boiling heat transfer of water on a superhydrophilic aluminum surface, in: ASME 2016 International Mechanical Engineering Congress and Exposition, ASME, Phoenix, USA, 2016.
[81] Y. Katto, Critical heat flux, Int. J. Multiphase Flow 20 (1994) 53–90.
[82] Y. Katto, S. Yokoya, M. Yasunaka, Mechanism of boiling crisis and transition boiling in pool boiling, in: 4th International Heat Transfer Conference, Begel House Inc., Paris-Versailles, France, 1970.
[83] V.I. Deev, V.E. Keilin, I.A. Kovalev, A.K. Kondratenko, V.I. Petrovichev, Nucleate and film pool boiling heat transfer to saturated liquid helium, Cryogenics 17 (1977) 557–562.
[84] D.N. Lyon, P.G. Kosky, B.N. Harman, Nucleate boiling heat transfer coefficients and peak nucleate boiling fluxes for pure liquid nitrogen and oxygen on

horizontal platinum surfaces from below 0.5 atmosphere to the critical pressures, in: K.D. Timmerhaus (Ed.), Advances in Cryogenic Engineering, Springer, New York, 1964, pp. 77–87.
[85] D.A. Labuntsov, V.V. Jagov, A.K. Gorodov, Critical heat fluxes in boiling at low pressure region, in: Proceedings of the 6th International Heat Transfer Conference, Toronto, Canada, 1978, pp. 221–225.
[86] Y. Shirai, H. Tatsumoto, M. Shiotsu, K. Hata, H. Kobayashi, Y. Naruo, Y. Inatani, Boiling heat transfer from a horizontal flat plate in a pool of liquid hydrogen, Cryogenics 50 (2010) 410–416.
[87] V.K. Dhir, Boiling heat transfer, Annu. Rev. Fluid Mech. 30 (1998) 365–401.
[88] L. Wang, Y. Li, F. Zhang, F. Xie, Y. Ma, Correlations for calculating heat transfer of hydrogen pool boiling, Int. J. Hydrogen Energy 41 (2016) 17118–17131.
[89] R.I. Soziev, M.A. Khrizolitova, Calculating critical heat flux density with pool boiling, Therm. Eng. 37 (1989) 400–401.
[90] H. Sakashita, Critical heat flux on a vertical surface in saturated pool boiling at high pressures, J. Therm. Sci. Technol. 11 (2016) 16–00264.
[91] V.M. Borishanskii, On the Problem of Generalizing Experimental Data on the Cessation of Bubble Boiling in Large Volume of Liquids, Report No. Ts. K.I.T 28, Moscow, Soviet Union, 1955.
[92] R. Moissis, P.J. Berenson, On the hydrodynamic transitions in nucleate boiling, J. Heat Transfer 85 (1963) 221–226.
[93] B.J. Kim, J.H. Lee, K.D. Kim, Improvements of critical heat flux models for pool boiling on horizontal surfaces using interfacial instabilities of viscous potential flows, Int. J. Heat Mass Transfer 93 (2016) 200–206.
[94] S.H. Yang, W.-P. Baek, S.H. Chang, Pool-boiling critical heat flux of water on small plates: effects of surface orientation and size, Int. Commun. Heat Mass Transfer 24 (1997) 1093–1102.
[95] I.I. Gogonin, S.S. Kutateladze, Critical heat flux as a function of heater size for a liquid boiling in a large enclosure, J. Eng. Phys. 33 (1977) 1286–1289.
[96] Y.H. Kim, S.J. Kim, J.J. Kim, S.W. Noh, K.Y. Suh, J.L. Rempe, F.B. Cheung, S.B. Kim, Visualization of boiling phenomena in inclined rectangular gap, Int. J. Multiphase Flow 31 (2005) 618–642.
[97] A. Priarone, Effect of surface orientation on nucleate boiling and critical heat flux of dielectric fluids, Int. J. Therm. Sci. 44 (2005) 822–831.
[98] M.S. El-Genk, H. Bostanci, Saturation boiling of HFE-7100 from a copper surface, simulating a microelectronic chip, Int. J. Heat Mass Transfer 46 (2003) 1841–1854.
[99] M. El-Genk, H. Bostanci, Combined effects of subcooling and surface orientation on pool boiling of HFE-7100 from a simulated electronic chip, Exp. Heat Transfer 16 (2003) 281–301.
[100] C. Beduz, R.G. Scurlock, A.J. Sousa, Angular dependence of boiling heat transfer mechanisms in liquid nitrogen, in: R.W. Fast (Ed.), Advances in Cryogenic Engineering, Springer, New York, 1988, pp. 363–370.
[101] M.J. Brusstar, H. Merte, R.B. Keller, B.J. Kirby, Effects of heater surface orientation on the critical heat flux—I. An experimental evaluation of models for subcooled pool boiling, Int. J. Heat Mass Transfer 40 (1997) 4007–4019.
[102] H. Sakashita, A. Ono, J. Nyui, Critical heat flux and near-wall boiling behaviors in saturated and subcooled pool boiling on vertical and inclined surfaces, J. Nucl. Sci. Technol. 46 (2009) 1038–1048.
[103] A.H. Howard, I. Mudawar, Orientation effects on pool boiling critical heat flux (CHF) and modeling of CHF for near-vertical surfaces, Int. J. Heat Mass Transfer 42 (1999) 1665–1688.
[104] C.-K. Guan, J.F. Klausner, R. Mei, A new mechanistic model for pool boiling CHF on horizontal surfaces, Int. J. Heat Mass Transfer 54 (2011) 3960–3969.
[105] I.P. Vishnev, Effect of orienting the hot surface with respect to the gravitational field on the critical nucleate boiling of a liquid, J. Eng. Phys. Thermophys. 24 (1973) 43–48.
[106] M. Arik, A. Bar-Cohen, Ebullient cooling of integrated circuits by Novec fluids, in: Proceedings of the Pacific Rim International Intersociety Electronic Packaging Conference, Hawaii, USA, 2001.
[107] J.Y. Chang, S.M. You, Heater orientation effects on pool boiling of micro-porous-enhanced surfaces in saturated FC-72, J. Heat Transfer 118 (1996) 937–943.
[108] M.S. El-Genk, Z. Guo, Transient boiling from inclined and downward-facing surfaces in a saturated pool, Int. J. Refrig. 16 (1993) 414–422.
[109] M.J. Brusstar, H. Merte, Effects of heater surface orientation on the critical heat flux–II. A model for pool and forced convection subcooled boiling, Int. J. Heat Mass Transfer 40 (1997) 4021–4030.
[110] M.J. Brusstar, H. Merte Jr., Effects of buoyancy on the critical heat flux in forced convection, J. Thermophys. Heat Transfer 8 (1994) 322–328.
[111] R.F. Gaertner, Photographic study of nucleate pool boiling on a horizontal surface, J. Heat Transfer 87 (1965) 17–27.
[112] Y. Katto, S. Yokoya, Principal mechanism of boiling crisis in pool boiling, Int. J. Heat Mass Transfer 11 (1968) 993–1002.
[113] I.C. Bang, S.H. Chang, W.-P. Baek, Visualization of a principle mechanism of critical heat flux in pool boiling, Int. J. Heat Mass Transfer 48 (2005) 5371–5385.
[114] H. Sakashita, T. Kumada, A new model for CHF in pool boiling at higher pressure, JSME Int. J. Ser. B 36 (1993) 422–428.
[115] A.K. Rajvanshi, J.S. Saini, R. Prakash, Investigation of macrolayer thickness in nucleate pool boiling at high heat flux, Int. J. Heat Mass Transfer 35 (1992) 343–350.
[116] P. Sadasivan, P.R. Chappidi, C. Unal, R.A. Nelson, Possible mechanisms of macrolayer formation, Int. Commun. Heat Mass Transfer 19 (1992) 801–815.
[117] T. Kumada, H. Sakashita, Pool boiling heat transfer–II. Thickness of liquid macrolayer formed beneath vapor masses, Int. J. Heat Mass Transfer 38 (1995) 979–987.
[118] H. Sakashita, A. Ono, Boiling behaviors and critical heat flux on a horizontal plate in saturated pool boiling of water at high pressures, Int. J. Heat Mass Transfer 52 (2009) 744–750.
[119] P.R. Chappidi, C. Unal, K.O. Pasamehmetoglu, R.A. Nelson, On the relationship between the macrolayer thickness and the vapor-stem diameter in the high-heat-flux, pool nucleate boiling region, Int. Commun. Heat Mass Transfer 18 (1991) 195–205.
[120] Y.-H. Zhao, T. Masuoka, T. Tsuruta, Unified theoretical prediction of fully developed nucleate boiling and critical heat flux based on a dynamic microlayer model, Int. J. Heat Mass Transfer 45 (2002) 3189–3197.
[121] S. Nishio, T. Gotoh, N. Nagai, Observation of boiling structures in high heat-flux boiling, Int. J. Heat Mass Transfer 41 (1998) 3191–3201.
[122] H.S. Ahn, M.H. Kim, Visualization study of critical heat flux mechanism on a small and horizontal copper heater, Int. J. Multiph. Flow 41 (2012) 1–12.
[123] B. Xiao, B. Yu, A fractal model for critical heat flux in pool boiling, Int. J. Therm. Sci. 46 (2007) 426–433.
[124] J. Jung, S.J. Kim, J. Kim, Observations of the critical heat flux process during pool boiling of FC-72, J. Heat Transfer 136 (2014) 041501.
[125] V.V. Yagov, A physical model and calculation formula for critical heat fluxes with nucleate pool boiling of liquids, Therm. Eng. 35 (1988) 333–339.
[126] H.J. Chung, H.C. No, A nucleate boiling limitation model for the prediction of pool boiling CHF, Int. J. Heat Mass Transfer 50 (2007) 2944–2951.
[127] S.J. Ha, H.C. No, A dry-spot model of critical heat flux in pool and forced convection boiling, Int. J. Heat Mass Transfer 41 (1998) 303–311.
[128] S.J. Ha, H.C. No, A dry-spot model of critical heat flux applicable to both pool boiling and subcooled forced convection boiling, Int. J. Heat Mass Transfer 43 (2000) 241–250.
[129] H.J. Van Ouwerkerk, Burnout in pool boiling the stability of boiling mechanisms, Int. J. Heat Mass Transfer 15 (1972) 25–34.
[130] T.G. Theofanous, J.P. Tu, A.T. Dinh, T.-N. Dinh, The boiling crisis phenomenon: Part I: nucleation and nucleate boiling heat transfer, Exp. Therm. Fluid Sci. 26 (2002) 775–792.
[131] T.G. Theofanous, T.-N. Dinh, High heat flux boiling and burnout as microphysical phenomena: mounting evidence and opportunities, Multiph. Sci. Technol. 18 (2006) 251–276.
[132] S.V. Gupta, Capillary action in narrow and wide tubes–a unified approach, Metrologia 41 (2004) 361–364.
[133] I.-C. Chu, H.C. No, C.-H. Song, D.J. Euh, Observation of critical heat flux mechanism in horizontal pool boiling of saturated water, Nucl. Eng. Des. 279 (2014) 189–199.
[134] J.Y. Choi, H.C. No, J. Kim, Development of a dry patch model for critical heat flux prediction, Int. J. Heat Mass Transfer 100 (2016) 386–395.
[135] D.E. Kim, J. Song, H. Kim, Simultaneous observation of dynamics and thermal evolution of irreversible dry spot at critical heat flux in pool boiling, Int. J. Heat Mass Transfer 99 (2016) 409–424.
[136] I.-C. Chu, H.C. No, C.-H. Song, Visualization of boiling structure and critical heat flux phenomenon for a narrow heating surface in a horizontal pool of saturated water, Int. J. Heat Mass Transfer 62 (2013) 142–152.
[137] J.E. Galloway, I. Mudawar, CHF mechanism in flow boiling from a short heated wall–I. Examination of near-wall conditions with the aid of photomicrography and high-speed video imaging, Int. J. Heat Mass Transfer 36 (1993) 2511–2526.
[138] J.E. Galloway, I. Mudawar, CHF mechanism in flow boiling from a short heated wall–II. Theoretical CHF model, Int. J. Heat Mass Transfer 36 (1993) 2527–2540.
[139] D. Zhong, J.a. Meng, Z. Li, Z. Guo, Critical heat flux for downward-facing saturated pool boiling on pin fin surfaces, Int. J. Heat Mass Transfer 87 (2015) 201–211.
[140] H. Zhang, I. Mudawar, M.M. Hasan, Experimental assessment of the effects of body force, surface tension force, and inertia on flow boiling CHF, Int. J. Heat Mass Transfer 45 (2002) 4079–4095.
[141] H. Zhang, I. Mudawar, M.M. Hasan, Flow boiling CHF in microgravity, Int. J. Heat Mass Transfer 48 (2005) 3107–3118.
[142] C. Konishi, I. Mudawar, Review of flow boiling and critical heat flux in microgravity, Int. J. Heat Mass Transfer 80 (2015) 469–493.